DOT/FAA/AR-95/76

Office of Aviation Research
Washington, D.C. 20591

Corrosion and Corrosion Fatigue of Airframe Materials

February 1996

Final Report

U.S. Department of Transportation
Federal Aviation Administration

DISCLAIMER NOTICE

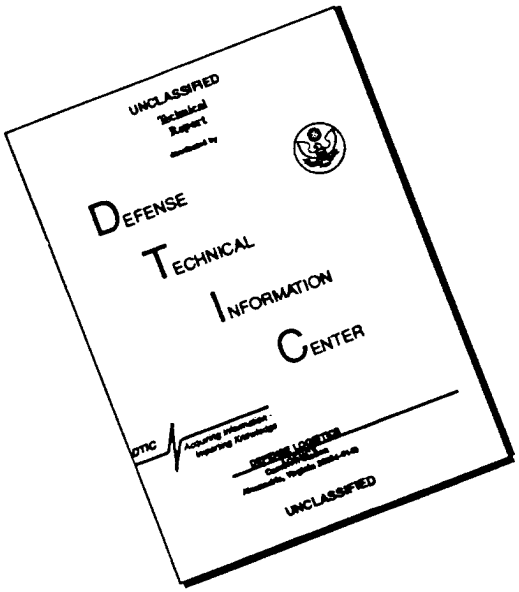

THIS DOCUMENT IS BEST QUALITY AVAILABLE. THE COPY FURNISHED TO DTIC CONTAINED A SIGNIFICANT NUMBER OF PAGES WHICH DO NOT REPRODUCE LEGIBLY.

NOTICE

Technical Report Documentation Page

1. Report No.	2. Government Accession No.	3. Recipient's Catalog No.
DOT/FAA/AR-95/76		

4. Title and Subtitle	5. Report Date
CORROSION AND CORROSION FATIGUE OF AIRFRAME MATERIALS	February 1996
	6. Performing Organization Code: LU Account No. 537717

7. Author(s)	8. Performing Organization Report No.
Robert P. Wei, D. Gary Harlow	

9. Performing Organization Name and Address	10. Work Unit No. (TRAIS)
Lehigh University Department of Mechanical Engineering and Mechanics 19 Memorial Drive West Bethlehem, PA 18015	
	11. Contract or Grant No.: 92-G-0006

12. Sponsoring Agency Name and Address	13. Type of Report and Period Covered
U.S. Department of Transportation Federal Aviation Administration Office of Aviation Research Washington, D.C. 20591	Final Report
	14. Sponsoring Agency Code: AAR-430

15. Supplementary Notes

FAA Technical Center Program Manager: Dr. Thomas Flournoy

16. Abstract

In support of the National Aircraft Research Program of the Federal Aviation Administration (FAA), Lehigh University undertook a multidisciplinary program of research to study corrosion and corrosion fatigue of airframe materials. The program is complemented by a program sponsored by the Air Force Office of Scientific Research (AFOSR). The objectives of these programs are (1) the development of basic understanding of the processes of localized corrosion and corrosion fatigue crack nucleation and growth in high-strength aluminum alloys used in airframe construction, (2) the formulation of kinetic models for these elemental processes, and (3) the integration of these models into probabilistic models that can provide guidance in formulating methodologies for service-life prediction.

This report summarizes research performed under the FAA sponsored (Phase I) program for the period from 15 June 1992 to 14 June 1995. Experimental efforts during this period were focused upon (1) characterizations of the chemical, microstructural and statistical aspects of pitting corrosion, and upon the kinetics of pitting of 2024-T3 aluminum alloy in aqueous environments; (2) establishment of the criteria for the transition from pitting to corrosion fatigue crack growth (i.e., crack nucleation); and (3) studies of corrosion fatigue crack growth (particularly in its early stage, or the so-called chemically short regime). The modeling effort, which cuts across the FAA and AFOSR programs, included the development and demonstration of a mechanistically based probability approach for service-life prediction and the formulation of a probability model for particle-induced corrosion pit growth that pertains to multiple-site-damage (MSD) analysis.

17. Key Words	18. Distribution Statement
Corrosion, corrosion fatigue, localized corrosion, pitting, crack nucleation, fatigue crack growth, life prediction, probability modeling, airframe materials, aluminum alloy, 2024-T3 alloy	This document is available to the public through the National Technical Information Service (NTIS), Springfield, Virginia 22161.

19. Security Classif. (of this report)	20. Security Classif. (of this page)	21. No. of Pages	22. Price
Unclassified	Unclassified	55	

PREFACE

Individuals who have contributed to the Phase I effort include Dr. Robert P. Wei, Principal Investigator (fracture mechanics and materials science); Dr. D. Gary Harlow (probability modeling); Dr. Ming Gao (materials science); Dr. Gim-Syang Chen (corrosion and materials science); Dr. Richard Granata (corrosion); Dr. Hyacinth Vadage (corrosion); Dr. Jean Marc Olive, a Visiting Scientist from C.N.R.S at the Université de Bordeaux in France (material science); Mr. Ray Burynski (M.S. candidate in Applied Mechanics); Mr. Joseph Wan (Ph.D. candidate in Applied Mechanics); Mr. Chi-Min Liao (Ph.D. candidate in Materials Science and Engineering); and Ms. Nancy Cawley (Ph.D. candidate in Applied Mathematics). Mr. Liao is supported by his employer, China Steel Corporation in Taiwan, and Ms. Cawley (contributing to statistical modeling) is supported by the AFOSR program.

TABLE OF CONTENTS

LIST OF FIGURES

LIST OF TABLES

EXECUTIVE SUMMARY

In support of the National Aircraft Research Program of the Federal Aviation Administration (FAA), Lehigh University undertook a multidisciplinary program of research to study corrosion and corrosion fatigue of airframe materials. The program was initiated on 15 June 1992 (as Phase I) and has been extended to 15 June 1998 (as Phase II) and is complemented by a program sponsored by the Air Force Office of Scientific Research (AFOSR). The objectives of these programs are (1) the development of basic understanding of the processes of localized corrosion and corrosion fatigue crack nucleation and growth in high-strength aluminum alloys used in airframe construction, (2) the formulation of kinetic models for these elemental processes, and (3) the integration of these models into probabilistic models that can provide guidance in formulating methodologies for service-life prediction. Experimental efforts under the FAA-sponsored program are directed at the 2024-T3 aluminum alloy, while those under the AFOSR-sponsored program are concentrated on the 7075-T651 alloy.

This report summarizes research performed under the FAA-sponsored (Phase I) program for the period from 15 June 1992 to 14 June 1995. Experimental efforts during this period were focused upon (1) characterizations of the chemical, microstructural and statistical aspects of pitting corrosion, and upon the kinetics of pitting of 2024-T3 aluminum alloy in aqueous environments; (2) establishment of the criteria for the transition from pitting to corrosion fatigue crack growth (i.e., crack nucleation); and (3) studies of corrosion fatigue crack growth (particularly in its early stage, the so-called chemically short regime). The modeling effort, which cuts across the FAA and AFOSR programs, included the development and demonstration of a mechanistically based probability approach for service-life prediction and the formulation of a probability model for particle-induced corrosion pit growth that pertains to multiple-site-damage (MSD) analysis.

1. BACKGROUND AND OBJECTIVES.

Localized corrosion (in the form of exfoliation and pitting in aluminum alloys) and corrosion fatigue crack nucleation and growth are clearly recognized as degradation mechanisms that affect the durability and integrity of commercial transport aircraft. The Aloha incident, as well as studies by the airframe manufacturers (for example, the Aging Fleet Evaluation Program by Boeing [1]), indicate that corrosion is far more widespread than anticipated. A quantitative methodology for defining suitable inspection intervals and mandating repairs and for assessing the durability and integrity of airframe components is needed for the effective management of the nation's aging fleet of commercial transport aircraft. The development of such a methodology requires a quantitative understanding, characterization and modeling of the elemental processes of damage, and the integration of the various models into a suitable probabilistic framework for service-life prediction. Such an understanding of the damaging mechanisms and the formulation of a predictive methodology will also assist in the design of new aircraft and in the development of suitable "fixes" for the current fleet.

Lehigh University proposed to undertake a 3-year program of research to study corrosion and corrosion fatigue of airframe materials in support of the FAA Aging Airplane Program. The program was accepted by the FAA and research was initiated on 15 June 1992 (Phase I). This program has been extended to 15 June 1998 (as Phase II) and is complemented by a program sponsored by the Air Force Office of Scientific Research (AFOSR). The objectives of these programs are (1) the development of basic understanding of the processes of localized corrosion and corrosion fatigue crack nucleation and growth in high-strength aluminum alloys used in airframe construction, (2) the formulation of kinetic models for these elemental processes, and (3) the integration of these models into probabilistic models that can provide guidance in formulating methodologies for service-life prediction. Experimental efforts under the FAA-sponsored program are directed at the 2024-T3 aluminum alloy, while those under the AFOSR-sponsored program are concentrated on the 7075-T651 alloy. In this report, work performed under Phase I of the FAA-sponsored program is summarized. The modeling effort, which cuts across the FAA and AFOSR programs, is included in this summary report.

2. TECHNICAL APPROACH.

The development of damage is illustrated schematically in figure 1, and is shown in a flow diagram in figure 2. The early stage is dominated by corrosion in the form of pitting or exfoliation and the later stage by corrosion fatigue crack growth. Within the context of these mechanisms, an upper bound of damage is to be defined in terms of structural reliability and damage tolerance considerations for mandating repairs. The research is focused, therefore, on the quantitative understanding and characterization and kinetic modeling of the following elemental processes:

- Onset of localized corrosion damage (particularly, mechanisms and kinetics of pit nucleation and growth).
- Transition from pitting to fatigue crack growth.
- Early stages of corrosion fatigue crack growth (short-crack regime).

- Corrosion fatigue crack growth.

Formulation of a predictive model must include the probabilistic contributions from material properties and key variables on the rate of corrosion (particularly, pit nucleation and growth) and corrosion fatigue crack growth and on the transition from corrosion to cracking.

The principal issues being addressed are as follows:

- Identification and verification of key internal and external variables that control each of the aforementioned unit processes for corrosion and corrosion fatigue cracking and determination of the stochastic nature of each process.

- Quantification of the probability distribution function (including time variance) of each of the key variables.

- Development of a quantitative understanding of the rate controlling step and mechanism for each damage process and formulation of a mechanistic (*deterministic*) model for each that describes the functional dependence on the key variables.

- Integration of mechanistic models and probability distribution functions and formulation of mechanistically based probability models for life prediction and reliability assessment.

The concept of a competition between localized (*pitting*) corrosion and corrosion fatigue crack growth in high-strength aluminum alloys was confirmed by experimental observations early in the program [2]. In addition, the early experiments showed localized (*pitting*) corrosion to be associated with *constituent particles*, and pit growth appeared to result from the coalescence of pits formed in particle cluster. The particle density can be high (i.e., about 3,000 particles/mm^2 for those with projected surface area >1 μm^2). Clustering and banding were evident and appeared to depend on orientation. The research emphasis, therefore, was placed on the role of constituent particles on pitting corrosion and the transition to fatigue crack growth.

3. PARTICLE-INDUCED PITTING CORROSION.

Examinations of the process of localized corrosion was carried out on a 1.6-mm-thick bare 2024-T3 aluminum alloy sheet [3]. The chemical composition of this sheet was determined by spectroscopic and spectrochemical analyses and is given in weight percent (wt%) as follows: Cu77 4.24, Mg 1.26, Mn 0.65, Fe 0.15, Si 0.06, Zn 0.08, Ti 0.031, Cr <0.01, and Al balance. The as-received material was cut into 10- x 10-mm specimens for corrosion testing. The specimens were ground through a graded series of SiC papers and then polished with diamond paste and colloidal SiO_2 to achieve mirror-like flat surfaces (~0.05 μm rms surface roughness). After polishing, the specimens were cleaned with water and ethyl alcohol and dried with warm air. Prior to corrosion testing, each specimen was coated with stop-off lacquer so that only the polished surface would be exposed to the test environment. For these studies, 0.5M (molar) NaCl (sodium chloride) solution was used. The solution was prepared by mixing 29.22 gm (0.5 mole) of reagent grade sodium chloride crystals with deionized water to make one liter of solution. The corrosion experiment was performed by simply immersing the specimen in a covered glass jar containing 200 mL of 0.5M NaCl solution, with no applied potential, at the desired temperatures

(from 5 to 80°C) for various periods of time. Before corrosion testing, the solution pH was typically about 5.8 and the oxygen concentration was approximately 7 ppm. After testing for 24 hours at 80°C, for example, the pH increased slightly to 6.7 and the oxygen level dropped to 5.2 to 6.6 ppm.

Following corrosion, the corrosion products were chemically stripped from the exposed surface following the guidelines given in [4]. The stripping solution was prepared by adding 17.5 mL of phosphoric acid and 5 grams of chromic trioxide (CrO_3) to deionized water to make 1 L of solution. Stripping was accomplished by immersing the specimen into the stripping solution (maintained at approximately 60°C) for 5 min., followed by rinsing with deionized water, gently wiping off with an alcohol swab, and drying in air. The specimen was then stored in a desiccator prior to further examination. Trials were conducted and showed that the oxide stripping procedure did not cause further corrosion damage to the surface [2]. Scanning electron microscopy (SEM) and energy dispersive X-ray spectroscopy (EDX) were used to investigate the surface morphology and chemical composition of the alloy surface and constituent particles.

3.1 ROLE OF CONSTITUENT PARTICLES.

Figure 3 shows the same (representative) area of a polished surface before and after corrosion. The presence of a large number of constituent particles is evident. It is also clear that early corrosion is associated with these constituent particles. Some clustering of the particles is evident, and there is some banding of particles along the rolling direction of the sheet.

Typical SEM and EDX results for constituent particles are shown in figure 4. Two types of particles are noted; one of which (Particle A) contains Al, Cu and Mg, and the other (Particle C), Al, Cu, Fe and Mn. (The chromium and phosphorus peaks in the EDX spectra are from residual contaminations by the corrosion stripping solution.) These particles were formed during processing. Their differences in composition result in differences in electrochemical potential between the particle and the matrix, between individual particles and between areas within the individual particles, and can lead to localized galvanic corrosion [5,6]. The relatively active phases or regions dissolve and lead to pit nucleation.

Srivastava and Ives [5] proposed a number of processes in which constituent particles may nucleate pitting corrosion; namely, (i) the particle is unstable in the environment, but the matrix is relatively stable or covered by a protective film; (ii) certain phases of the particle are unstable, but the matrix is stable; (iii) the particle is cathodic to the matrix, causing preferential dissolution of the matrix adjacent to the particle; and (iv) the particle is debonded from the matrix, thereby forming an incipient crevice to initiate localized corrosion. In this context, the composition of constituent particles, their size, quantity, and distribution would be important in determining the pitting behavior of the alloy.

Figure 4 also shows typical corrosion associated with the constituent particles. Corrosion associated with the Al-Cu-Mg-containing particles (Particle A) suggests dissolution of the particles and possible corrosion of the matrix surrounding the particles. Trench-like crevices, on the other hand, surround the Al-Cu-Fe-Mn particles (Particle C) and suggest principally matrix dissolution. It is conceivable that localized corrosion readily takes place at particle/matrix interfaces since passive films at these regions have lower protective ability because of their

poorer structural integrity at the interface area and since the potential difference of the particle/matrix galvanic couple provides a strong chemical driving force for the anodic dissolution of the active phase. A clearer picture of the difference in corrosion associated with these particles is shown in figure 5.

The pitting morphologies of two adjacent particles with different compositions and the respective EDX spectra are shown in figure 6. The figure shows possible interactions between these dissimilar particles. The Fe-Mn-containing particle (Particle A) exhibited corrosion attack of the adjacent matrix. The Mg-containing particle (Particle B) is overlaid with a plating or deposit of Cu. Since Cu has the most noble electrochemical potential in this system, it is not surprising that the cupric cations resulting from the matrix dissolution of the 2024-T3 alloy can be converted back to copper by reduction reaction and deposit on the cathodic sites.

EDX results for selected constituent particles before and after corrosion testing are shown in table 1. It is clear that the Mg in all of the Al-Cu-Mg particles was removed by corrosion. There is some evidence of Fe and Mn deposition onto the Al-Cu-Mg particle sites during corrosion. The relative intensity of Al appeared to have decreased and that of Cu increased. The possible reasons for this phenomenon are (i) cathodic reduction of the noble elements on the top of the particle enhances the characteristic X-ray intensity of these elements but reduces the intensity of other active elements, and (ii) the constituent particles experienced dealloying, similar to that of brass. Since Mg and Al are electrochemically active relative to Cu and Fe, the latter hypothesis is more likely. In fact, dealloying of an intermetallic T_1 phase (Al_2CuLi) and dealuminization of γ_2 (Cu_2Al) compounds have been reported in the literature [7,8]. The data on the Fe-Mn-containing alloys are less clear because of Cu deposition on some of the particles. The SEM evidence suggests that these particles promoted dissolution of the adjacent matrix and did not undergo dissolution themselves.

It is clear that the bare 2024-T3 alloys corrode readily in 0.5M NaCl solution. The corrosion is promoted by the presence of constituent particles. The interactions between the particles and the matrix are complex and need to be understood as a part of the program in developing models for corrosion damage. It is recognized that the particle distribution is 3- dimensional in nature and would influence the growth of pits in depth as well as in breadth. No evidence of exfoliation was uncovered. Principal emphasis of the program, therefore, was placed on pitting corrosion.

3.2 CONSTITUENT PARTICLES.

On the basis of their corrosion behavior, the constituent particles may be separated into two types: Type A particles that are *anodic* and Type C particles that are *cathodic* with respect to the matrix. Type A particles are those that contain Al, Cu and Mg. They tended to be small and nearly equi-axed. Type C, on the other hand, are those with Al, Cu, Fe and Mn. These particles tend to be larger and are often elongated and aligned along the rolling direction. The density of these (Types A and C) particles in the LT (sheet) surface (with projected surface area greater than 1 μm^2) was estimated to be 3,000 particles/mm^2 for this 2024-T3 (bare) alloy sheet. The distributions in particle sizes are shown in figure 7. Elemental (EDX) maps showed that nearly 75% of the constituent particles in this 2024-T3 alloy sheet are Type A (i.e., anodic relative to the matrix).

These constituent particles were characterized by X-ray microprobe analysis and transmission electron microscopy (TEM). The particle composition, based on X-ray microprobe analyses, is given in table 2. Taken in conjunction with the TEM analyses, Type A particles were found to be principally $CuMgAl_2$. Type C particles, on the other hand, were identified with complex intermetallics of the type $(FeMnCu)(CuAl)_6$.

3.3 PITTING CORROSION.

To quantify the evolution of corrosion (pitting) damage and to examine the influences of solution pH, temperature and orientation on particle-induced pitting, more extensive corrosion tests were carried out [9,10]. The specific conditions are shown in the test matrix (table 3). The same area of a specimen surface, before and after corrosion, was examined by scanning electron microscopy for constituent particles and pit morphologies, and computer-aided image analyses of the SEM images were used to quantify pitting damage.

3.3.1 Size, Distribution, and Kinetics.

Figure 8 shows a representative area and typical corrosion damage following 72 hours of exposure to 0.5 M NaCl solution (exposed to air, with $[O_2]$ = 7 ppm and pH ≈ 6) at 65°C and confirms the important role played by the constituent particles in pitting corrosion. Corrosion attack associated with the particles (showing one-to-one correspondence between particles and pits) is readily seen (compare figures 8a and 8b). Particles that are predominantly cathodic with respect to the matrix promoted matrix dissolution at their periphery. Those that are predominantly anodic were themselves dissolved. Linkup of individual pits to form larger pits is also evident.

The evolution of particle-induced pitting on the rolling (LT) plane of a bare 2024-T3 alloy was characterized as functions of time and temperature from 5 to 65°C [9,10]. The severity of pitting was observed to increase with increasing exposure time and solution temperature. Type A particles being anodic simply dissolved themselves. Figures 9 and 10 show typical distributions of pit size as a function of exposure time at given temperatures (figure 9) and as a function of temperature at given exposure times (figure 10) [11]. Each set of data represents measurement from a separate specimen and is comprised of several hundred particle-induced pits.

The general trend of the data (figures 9 and 10) reflects the expected increasing rates of pit evolution or growth with increasing time and temperature. More detailed inspection shows, however, that changes in pit size are much more rapid for the larger pits; there was little or no change for the smaller pits. This trend is more clearly reflected by replotting the data from figure 10 at given percentile levels (see figure 11) and is interpreted in terms of the nature and distribution of the constituent particles. Because Type A (*anodic*) particles dissolve themselves, without significantly attacking the adjacent matrix, the pits that are produced simply represent an "emptying" of the volume originally occupied by the particles and, therefore, do not change with time (see figure 5a). Type C (*cathodic*) particles, on the other hand, promote dissolution of the matrix and, hence, growth and link up with their neighbors to form a larger pit (see figure 5b). Because Type A particles tend to be smaller, they would dominate the lower end of the distribution; i.e., accounting for nearly all of the smaller particles even though the overall ratio of Type A to Type C particles is 3:1. Similarly, the upper end of the distribution would be dominated by the larger Type C particles.

Since fatigue cracks are expected to nucleate from the larger pits, an examination of pitting response was made in terms of the largest fifteen pits from the data shown in figures 9 and 10. By assuming a hemispherical shape for the pits and the originating particles, changes in volume with time were estimated at different test temperatures and are shown in figure 12. The scatter in data reflects variability in the size of particle clusters, specimen-to-specimen variability, and sampling errors. Growth of these larger pits appears to follow Faradaic law; i.e., exhibiting constant volumetric dissolution rates or a linear dependence of volume change on time (figure 12). Using the linear time dependence, the data are normalized (or pooled) and shown in an Arrhenius plot in figure 13. An activation energy for pit growth was estimated to be 39 ± 6 kJ/mol. This value is consistent with 50 kJ/mol that had been estimated for pit initiation[12].

A comparison of the largest pit found on the rolling (LT) surface with those for fatigue crack nucleation from the open-hole specimens (i.e., the thickness orientation or SL/ST surfaces) suggests that local corrosion sensitivity is orientation dependent. Pitting was *more severe in the thickness orientation*, with the largest pit 5 times larger in radius, or 100X in volume, than that on the rolling plane. Pitting was found to be very complex and involved 3-D interactions with constituent particles. Severe pitting is tentatively identified with clusters of particles containing a large number of Type C (*cathodic*) particles, with pit growth facilitated by channels opened by matrix dissolution around the Type C particles (see subsection 3.3.3).

3.3.2 Influences of pH.

The influences of solution and temperature on the evolution of pitting damage were examined. The effect of solution pH was investigated by performing corrosion tests at room temperature for three days in 0.5M NaCl solutions with pH = 3 and pH = 11, respectively. These results are compared against corresponding tests at pH ≈ 6. Figure 14 shows that the alloy experienced only limited pitting at pH = 3 (see figure 14a). SEM micrograph at a higher magnification (figure 14b) indicated that, in this acidic NaCl solution, anodic particles dissolved readily while the matrix surrounding the cathodic particles experienced very slight local attack. Exposure to the alkaline NaCl solution (pH = 11), on the other hand, resulted in significant corrosion attack of the sample surface. Detailed pitting features could not be clearly identified with the constituent particles (figure 15a). Instead, very large cavities (as compared to individual particles) were evident (figure 15b). McKee and Brown [13] showed that regardless of the presence or absence of chloride ions, aluminum was significantly attacked in NaOH solution at concentrations above 0.0005M but was resistant to ammonium hydroxide (NH_4OH) even at 10M. Their findings indicate the importance of certain cations, in addition to the solution pH, in determining the solubility of the aluminum oxide film. Understanding of the mechanisms and the implications of pH effect on corrosion in aging aircraft require further examination and will be continued under the Phase II program.

3.3.3 General and Severe Pitting/Orientation Dependence.

The results for the rolling plane (subsection 3.3.1) showed that the process is very complex and involves 3-D interactions with constituent particles. Corrosion sensitivity appears to be orientation dependent; it being *more severe in the thickness orientation* (the orientation that is more representative of the surface of a rivet or fastener hole) because of local segregation of constituent particles. To provide additional insight in understanding micro-constituent-induced localized corrosion, pitting of the transverse sections of 2024-T3 (bare) alloy at room temperature was studied by *in-situ* monitoring with a stereo video microscope system. Scanning electron microscopy (SEM) and energy dispersive spectroscopy (EDX) were then used to characterize the pitted specimens.

Two modes of pitting corrosion are now clearly identified: (i) ***general*** pitting over the specimen surface, and (ii) ***severe*** localized pitting at selected sites. General pitting occurs almost immediately upon specimen immersion and leads to the formation of small, shallow pits over the entire specimen surface. Each pit is clearly identified with a constituent particle on the specimen surface with particle or matrix dissolution determined by the nature (anodic or cathodic) of the particle. Severe localized pitting occurs at selected sites resulting in larger and deeper pits. Figure 16 shows typical surfaces of specimens after corrosion, and after cleaning by dry stripping. The areas of severe localized pitting are covered with a heavy layer of corrosion product. The density of severe localized pits was about 1 pit/mm^2 following 500-hour exposure, *versus* about 3,000 pits/mm^2 for general pitting.

Nucleation of severe localized pitting at individual sites involved an incubation time, which varied from tens of minutes to many hours (as short as 15 min. to over 30 hours during a 500-hour-long test), figure 17. The existence of an incubation period implied the need for local "breakdown" or corrosion at the surface as a precursor for subsequent subsurface attack. Severe localized pitting was always accompanied by gas evolution, which indicated strong electrochemical reactions within the pits. As pitting proceeded, corrosion products gradually accumulated around the pits, eventually covering the entire pitting region to form an occluded cell under which pitting continued to proceed. Severe localized pitting is believed to result from interactions of the matrix with ***a cluster or clusters*** of subsurface constituent particles, which formed local galvanic cells to sustain continued dissolution. Figure 17 shows such clusters of constituent particles within the large pits (see particularly inset to figure 17). The particles in the cluster are rich in Fe and Mn, i.e., of Type C (or cathodic). A conceptual model for pit growth associated with a cluster of particles is depicted in figure 18.

These findings confirm the original postulate for particle-induced pitting in these aluminum alloys. General pitting is typically associated with an individual (or, at most, a few) particles at the surface. It occurs almost immediately upon exposure to the aqueous solution and tends to stop once the particle dissolves or its contact with the matrix is undermined by corrosion. Severe localized pitting, on the other hand, involves a cluster or clusters of particles. The multiparticle interactions within a pit (or occluded region surrounding the pit), however, make the problem much more challenging. Because this severe localized pitting is clearly linked to corrosion fatigue crack nucleation, these efforts are being continued under the Phase II program to develop further mechanistic understanding and modeling of this process.

3.4 STATISTICAL CHARACTERIZATION AND MODELING OF THE SPATIAL DISTRIBUTION OF CONSTITUENT PARTICLES.

Because particle-induced pitting has been identified as the precursor for corrosion fatigue crack growth, information on the spatial distribution of constituent particles and the ability to *estimate* the probability for encountering a certain size or group of particles becomes important to a mechanistically based probability method for life prediction. This effort is focused, therefore, on the characterization and statistical modeling of the spatial distributions (relative locations and sizes) of these particles in the alloy, prior to and during pitting corrosion [14].

Extensive data analysis has confirmed that the particles, especially the cathodic ones, tend to be clustered. On the rolling (LT) surface a more regular pattern is apparent after corrosion, if all particles are considered. A schematic representation of the spatial pattern of particles before corrosion is shown in figure 19. This diagram was generated by using a circular disk, with an area equal to the particle area about its centroid, to represent each of the particles (compare figures 19 and 20). Since the spatial distribution of the particles is a geometrically dependent stochastic process, advanced estimation techniques using the first and second order properties of spatial point processes were also used to examine the data. Figure 21 is a plot of the second order properties, which confirms the clustering of particles and the fact that the distribution of particle-induced pits become more regular as corrosion progresses.

Recognizing that the particles may be anodic or cathodic and that they respond differently during corrosion, further efforts have been directed at characterizing and modeling precisely the spatial distribution of each type of particles. Since the anodic particles tend to dissolve relatively rapidly, the induced pits typically are the same size as the anodic particle, and they rarely contribute to the initiation of severe damage. However, the cathodic particles appear to continue to drive local corrosion until the induced pits are considerably larger than the cathodic particles. In addition, the local corrosion often progresses to include interactions between several cathodic particles. Thus, particular attention is being given to characterize and model the clustering of particles, especially cathodic ones, in the alloy (including the number, size, shape, and chemical composition of the particles in the clusters).

By considering twelve distinct polished sections of 2024-T3 with optical microscopy, a total of 1,596 cathodic particles were observed. The following illustrates some of the statistical analyses for the observations. The aspect ratios of the polished sections of the cathodic particles range from 1.00 to 4.72 with a mean of 1.57. Thus, the cross sections of the cathodic particles are more elliptical than circular. The nearest-neighbor cumulative distribution function (CDF) for the cathodic particles can be estimated by a two parameter Weibull CDF with a shape parameter of 1.8 and a scale parameter of 42.3 μm. Thus, the mean nearest-neighbor distance is 37.7 μm. To estimate the frequency of the number of cathodic particles per cluster, a definition for the cluster is required. It was assumed that any two particles are within the same cluster if the distance between their centroids is less than 37.7 μm. Under this condition, the frequency can be approximated by the following Pareto distribution [15]:

$$p_k = \Pr\{\text{number of cathodic particles per cluster} = k\} = 0.725k^{-2.41},\ k \geq 1.$$

4. TRANSITION FROM PITTING TO FATIGUE.

Corrosion fatigue failures often result from the nucleation and growth of fatigue cracks from corrosion induced pits [16,17]. Cracking occurs when the local mechanical condition is adequate for the onset of crack growth. Kondo [18] considered the competition between corrosion pit and fatigue crack growth in steels and proposed a criterion for the transition from pitting to corrosion fatigue crack growth, figure 1. The criterion is based on the assumption that a corrosion pit may be modeled by an equivalent semielliptical surface crack. It suggests that transition from pit growth to fatigue crack growth takes place when the stress intensity factor of the equivalent surface crack reaches the threshold stress intensity factor (ΔK_{th}) for fatigue crack growth. Through this criterion a linkage is made between the critical pit size (for a given applied stress) and a fracture mechanics parameter to provide a framework for the prediction of pitting/corrosion fatigue life.

To assess the applicability of this criterion for aluminum alloys, specimens containing a 6.35-mm-diameter central hole were tested in fatigue at an applied σ_{max} = 103.5 MPa (or $(\sigma_{max})_{hole}$ = 320 MPa), R = 0.1 and different loading frequencies at room temperature in a 0.5M NaCl solution (exposed to air, with pH ≈ 6). Cracks were found to nucleate from areas of severe local corrosion (*pits*), figures 22-26. Fatigue failure, by and large, resulted from a *single* nucleation site. Hence, a dominant flaw model for corrosion and corrosion fatigue appears to be appropriate. The process of early fatigue crack growth from a very complex corrosion pit to a well-developed crack front that is readily identified by conventional scanning electron microscopy (figure 22) was reconstructed by Kobayashi [19] using FRASTA. The successful reconstruction provides further support for the concept of the nucleation of fatigue cracking from a dominant corrosion pit.

In contrast to the original concept of Kondo et al. [18,20], however, the pit-to-crack transition size (or crack nucleation size) appears to depend on the cyclic-load frequency being larger at lower frequencies (*cf.* figures 22 and 24). This frequency dependence reflected *competition* between pitting corrosion and fatigue. The addition of a growth rate requirement to the transition criterion, therefore, is needed; namely,

$$\Delta K \geq \Delta K_{th}$$

$$(da/dt)_{crack} \geq (da/dt)_{pit}$$

where ΔK_{th} is the threshold for fatigue crack growth, and (da/dt) refers to the appropriate crack and pit growth rates (see figure 1). The rate criterion was added to the threshold criterion of Kondo et al. [18,20] to ensure that the fatigue crack, once nucleated, can outpace the concomitant corrosion. The need for the additional criterion is reflected by the data in figure 27, showing the crack size (or equivalent pit size) at nucleation (or transition) as a function of 1/frequency.

The possible influence of applied stress on the transition criteria was investigated. Experiments were conducted at lower stress levels ($(\sigma_{max})_{hole}$ = 144, 192, and 288 MPa). The results are summarized in figure 28. The transition ΔK results suggested that there was no significant influence of applied stress. Because of the much slower rate of fatigue crack growth at the lower stress levels, the times in solution (and to crack "nucleation") and the transition pit sizes were

stress levels, the times in solution (and to crack "nucleation") and the transition pit sizes were much larger. Figure 28 shows that the transition pit size depended principally on the time in solution (which is very short at a fatigue frequency of 10 Hz); this dependence reflects the combined set of criteria.

The presence of extensive localized corrosion (pitting) on the fatigue fracture surfaces may be seen in figures 23, 25, and 26. The extent of pitting depended on frequency, which suggested that the pitting is the result of postcrack-growth corrosion and depended on the duration of exposure of the fracture surface to the electrolyte. The presence of postcrack growth further confirmed the competition between corrosion and fatigue and argued against a dissolution based (versus hydrogen embrittlement) mechanism for crack growth.

5. FATIGUE CRACK GROWTH (SHORT-CRACK REGIME).

The influence of crack length on fatigue crack growth was examined. To distinguish between microstructurally short, mechanically short, and chemically short cracks and to develop mechanistic understanding of chemically short cracks, fatigue crack growth experiments were conducted under constant ΔK control in high-purity oxygen and aerated (with $[O_2]$ of 7 ppm) and deaerated 0.5M NaCl solution at room temperature. A single-edge-crack specimen was used to cover a range of crack lengths from 0.5 to 15 mm (or crack length-to-specimen width ratio of nearly zero to about 0.5).

Data for tests at ΔK of 5 and 10 MPa$\sqrt{m}$ (with R = 0.1) are shown in figure 29. Data in oxygen at both ΔK levels show independence of crack length and suggest that cracks longer than 0.5 mm are microstructurally and mechanically long. In other words, the crack response may be modeled in terms of (small-scale yielding) continuum mechanics. Data at ΔK = 5 MPa$\sqrt{m}$ for R = 0.1 and 0.5 (not shown) showed a significant effect of crack length out to about 4 mm in the *aerated* solution. No effect was observed, however, at ΔK = 5 MPa$\sqrt{m}$ (R = 0.1) in the deaerated solution and none at ΔK = 10 MPa$\sqrt{m}$ (R = 0.1) in either solution.

To better understand short crack growth in the 2024-T3 alloy, additional experiments were conducted in deaerated and aerated (with $[O_2]$ of 7 and 30 ppm) 0.5M NaCl solutions at ΔK of 4 to 10 MPa$\sqrt{m}$, R = 0.1. The results are shown along with the earlier data in figure 30. In agreement with the experiments at ΔK of 5 and 10 MPa$\sqrt{m}$, chemically short crack growth response was absent in the deaerated solution over the entire range of ΔK. The presence of chemically short crack growth response in the aerated 0.5M NaCl solutions, however, was found to depend on oxygen concentration and ΔK level. For $[O_2]$ of 7 ppm, the effect was present at ΔK below 6 MPa$\sqrt{m}$, R = 0.1. At an $[O_2]$ of 30 ppm, the effect, however, persisted to a ΔK of 8 MPa$\sqrt{m}$. The extent of the chemically short regime appears to depend on ΔK and $[O_2]$ and ranges from about 4 to 8 mm.

The existence of a chemically short regime over about 4 to 8 mm of growth is important in that the increased rate would promote earlier transition from pitting to fatigue cracking and reduce fatigue crack growth life. Comparison between the lower ΔK data in aerated and deaerated solutions suggested dissolved oxygen as an important contributor to the chemical effect. The dependence on ΔK, however, suggests the need for a more complex mechanistic explanation which would incorporate interactions between the environmental and loading variables. Further

studies are being carried out under the Phase II program to better understand and model this phenomenon.

6. PROBABILITY MODELING.

It was recognized that a quantitative methodology for life prediction is needed to help define suitable inspection intervals and assess the durability and integrity of aircraft components and structures. To be effective, this methodology must provide statistically accurate estimates of response for conditions not included within the available experimental observations and account for the influences of key external and internal variables. The external variables include applied stress $\Delta\sigma$, environmental chemistry, and temperature T; and the internal variables include chemistry within a pit or at the crack tip (for example), material properties, initial defect size, etc. (see figure 31). The development of such a methodology requires mechanistic understanding and quantification of the processes for damage accumulation. In other words, a mechanistically-based probability approach to life prediction (or durability assessment) is needed. The feasibility of this approach was first demonstrated for pitting and corrosion fatigue crack growth using a dominant flaw model, and it is being extended to the consideration of distribution in pit sizes in multiple-site-damage (MSD) analysis. Results from these efforts are briefly summarized below.

6.1 A MECHANISTICALLY BASED PROBABILITY APPROACH TO LIFE PREDICTION.

To demonstrate the feasibility and utility of this approach, a dominant flaw, probability model for pitting and corrosion fatigue was formulated [21]. This model was based on an original model proposed by Kondo [18] which assumed pitting corrosion at a constant volumetric rate. Transition from pit (hemispherical) to crack (semicircular) was based on a matching of the stress intensity factor for an equivalent semicircular crack against the fatigue crack growth threshold. A power-law model was used to represent subsequent fatigue crack growth. The constituent models were assumed to capture some of the key mechanistic features and provide reasonable "predictions" of response. The overall model incorporated initial defect size a_o, pitting current coefficient I_{Po}, fatigue crack growth rate coefficient C_c, and fatigue crack growth threshold (ΔK_{th}) as random variables. Specifically, the time to failure was found to be [21]:

$$t_f = \frac{2(\sqrt{\pi})^3\left[(\sqrt{\pi}\,\Delta K_{th}/2.2\Delta\sigma)^{-1} - \left(\sqrt{a_f}\right)^{-1}\right]}{\nu C_c(2.2\Delta\sigma)^3} + \frac{2\pi nF\rho\exp[\Delta H/RT]}{3MI_{Po}}\left[(\sqrt{\pi}\,\Delta K_{th}/2.2\Delta\sigma)^6 - a_o^3\right]$$

where a_f is the final crack size, ν is the cycle frequency, ρ is the density, M is the molecular weight, n is the valence of the aluminum, ΔH is the activation energy, F is Faraday's constant,

and R is the universal gas constant. Thus, the model contains a variety of random and deterministic variables which are directly related to the time to failure. The advantage of this type of formulation is that explicit computations can be made and examinations of the contribution of each of these variables to the distribution in life are possible.

This model has been modified further to account for corrosion and fatigue from an open circular hole. The modification included a further transition from the semicircular crack at an open hole to a through-thickness crack, as illustrated in figure 1, and is described in [22]. Typical results showing the influences of loading frequency, applied stress, and temperature are shown in figure 32. These findings demonstrate the importance and efficacy of this approach. The study confirmed the need for adopting this approach in the formulation of meaningful design methodology and life management programs.

6.2 PROBABILITY MODELING OF PIT GROWTH.

To establish a basis for predicting structural response, particularly in relation to MSD analysis, probabilistic modeling of pit growth was initiated to focus on the role of particle clusters on pit growth. The goal is to estimate the cumulative distribution function (*CDF*) for the size of corrosion pits at a given time which can then be used in multisite damage analysis. The model incorporates the evolution of local damage at each particle and pit growth through interactions with neighboring particles and the alloy matrix and takes advantage of information on particle distribution described under sections 3.3 and 3.4.

Three plausible, simplified models were considered to represent the propagation of pitting from particle to particle within a cluster. The simplification involves assumptions regarding the shape and aspect ratio for a pit that would be formed from a cluster of particles (i.e., an ellipsoid with given diameter-to-depth ratio). The models are as follows: (i) constant aspect ratio, (ii) discrete time dependent aspect ratio, and (iii) continuous time dependent aspect ratio. The latter two are more realistic, but are more complex.

Numerical results were obtained for the simplest case (model (i)) to illustrate the process. The key random variables (RVS) for this model are the cluster size N_c, the initial pit size a_o, and the pitting current coefficient I_{Po}. Typical results are shown in figures 33 and 34. Figure 33 shows the distribution in pit size after a given exposure for different numbers of constituent particles in the cluster, whereas figure 34 depicts the evolution in size distribution with time for a given sized particle cluster. It should be noted that, although the numbers of particles in the clusters may be the same, the physical dimensions of the clusters are quite different. The predicted response appears to be reasonable. The distribution in pit sizes for a given exposure and an arbitrary time may be deduced by incorporating information on clustering (see section 3.4). Figure 35 is a plot of the normalized pit density. This density gives the frequency of pits which may occur in the high stress region of a collection of rivet holes which are considered in multisite damage problems. For details of the model development and analysis, see Harlow and Wei [23].

7. SUMMARY.

Research during this phase has provided mechanistic insight into the processes of localized (pitting) corrosion and of corrosion fatigue crack nucleation and early growth. A framework and methodology for mechanistically-based probability modeling of these processes has also been developed and demonstrated.

Experimental investigations on 2024-T3 aluminum alloy have confirmed the original postulate for constituent-particle induced pitting and the subsequent nucleation and growth of corrosion fatigue cracks from the larger pits at high-stress locations in this class of aluminum alloys. Two modes of pitting were identified: general and severe localized pitting. General pitting is typically associated with an individual (or at most a few) particles at the surface. It occurs almost immediately upon exposure to the aqueous solution and tends to stop once the particle dissolves or its contact with the matrix is undermined by corrosion. Severe localized pitting, on the other hand, involves a cluster or clusters of particles and can be as large as 300x500 μm. Because of the three-dimensional nature of the particle distribution, the severity of pitting is strongly dependent on orientation; being more severe in the thickness orientations. The pitting process was found to be thermally activated, with an activation energy of about 40 kJ/mol.

Corrosion fatigue cracks nucleated from one or more of the severe localized pits. The criteria for nucleation (i.e., transition from pitting to cracking) required (1) the equivalent stress intensity factor range ΔK to exceed the fatigue crack growth threshold ΔK_{th} and (2) the time-based fatigue crack growth rate to exceed the pit growth rate. Because of the dual requirements, the time and pit size at nucleation are dependent on the fatigue loading frequency.

The early stage of corrosion fatigue crack growth in aqueous environments was examined. A chemically short regime, in which the crack growth rate exceeded that of a long crack, was identified for aerated 0.5M NaCl solution. This regime extended over about 5 mm in crack length but was totally absent in deaerated solutions. The chemically short crack effect was found to depend on the concentration of dissolved oxygen in the solution and to be coupled to ΔK level.

The multiparticle interactions within a pit (or occluded region surrounding the pit) and the observed chemically short crack effects, however, make the problem much more challenging. Because the severe localized pitting is clearly linked to corrosion fatigue crack nucleation and the nucleation criteria are clearly influenced by the short-crack behavior, these efforts will be extended and continued under Phase II to develop further mechanistic understanding and modeling of these processes.

The modeling efforts during this phase concentrated on the development of the technical approach and analysis methodology. The feasibility for integrating mechanistic understanding and probability analysis for pitting and corrosion fatigue crack growth has been demonstrated. Methods for statistical and probabilistic analysis and modeling of localized corrosion, which involves clusters of constituent particles, has been developed. These methods will be further developed and refined under Phase II to incorporate new experimental observations that will be taken.

8. REFERENCES.

1. U.G. Goranson, and M. Miller, "Aging Jet Transport Structural Evaluation Programs," presented at the 15th Symposium of the International Committee on Aeronautical Fatigue (ICAF), June 21-23, 1989, Jerusalem, Israel.

2. G.S. Chen, M. Gao, and R.P. Wei, "Micro-Constituents Induced Pitting Corrosion in a 2024-T3 Aluminum Alloy," Corrosion, to appear December 1995.

3. G. S. Chen, M. Gao, D. G. Harlow, and R. P. Wei, "Corrosion and Corrosion Fatigue of Airframe Aluminum Alloys," FAA/NASA International Symposium on Advanced Structural Integrity Methods for Airframe Durability and Damage Tolerance, NASA Conference Publication 3274, Langley Research Center, Hampton, VA, 23681, September 1994, pp. 157-173.

4. American Society for Metals, Metals Handbook, Ninth Edition, Volume 5, Surface Cleaning, Finishing, and Coating, American Society for Metals, Metals Park, Oh., 1982, p. 579.

5. S.C. Srivastava and M.B. Ives, "Dissolutions of Inclusions in Low-Alloy Steel Exposed to Chloride Containing Environments," Corrosion, 11, 1987, p.687.

6. Metals Handbook, Vol. 13, 9th Ed., ASM International, Metals Park, OH, 1987, p.584.

7. R.G. Buchheit, Jr., J.P. Moran, and G.E. Stoner, "Localized Corrosion Behavior of Alloy 2090 - The Role of Microstructural Heterogeneity," Corrosion, 46, 1990, p.610.

8. P. Sury and H.R. Oswald, "On the Corrosion Behavior of Individual Phases Present in Aluminum Bronzes," Corrosion Sci., 12, 1972, p.77.

9. Raymond M. Burynski, Jr., "Corrosion Response of a 2024-T3 Alloy in 0.5M NaCl Solution," MS Thesis, Lehigh University, 1994.

10. Raymond M. Burynski, Jr., Gim-Syang Chen, and Robert P. Wei, "Evolution of Pitting Corrosion in a 2024-T3 Aluminum Alloy," 1995 ASME International Mechanical Engineering Congress and Exposition on Structural Integrity in Aging Aircraft, San Francisco, CA, 47, C. I. Chang and C. T. Sun, eds., The American Society of Mechanical Engineers, New York, NY 10017, 1995, pp. 175-183.

11. K. Bury, Statistical Models in Applied Science, John Wiley and Sons, 1975, pp 367-371.

12. S. Dallek and R. T. Foley, "Mechanism of Pit Initiation on Aluminum Alloy Type 7075," J. of the Electrochemical Soc., 123, No. 12, pp. 1775-1779, December 1976.

13. A.B. McKee and R.H. Brown, "Resistance of Aluminum to Corrosion in Solutions Containing Various Anions and Cations," Corrosion, 3, 1947, p.595.

14. D. G. Harlow, N. R. Cawley and R. P. Wei, "Spatial Statistics of Particles and Corrosion Pits in 2024-T3 Aluminum Alloy," Proceedings of the 15th Canadian Congress of Applied Mechanics, B. Tabarrok and S. Dost, eds., May 28-June 2, 1995, Victoria, British Columbia, 1995, p. 116.

15. N. L. Johnson and S. Kotz, Discrete Distributions, John Wiley & Sons, New York, pp. 240, 1969.

16. D.W. Hoeppner, "Model for Prediction of Fatigue Lives Based upon a Pitting Corrosion Fatigue Process," in Fatigue Mechanisms, STP 675, ed., J.T. Fong, ASTM, Philadelphia, PA, 1979, p. 841.

17. M. Muller, "Theoretical Considerations on Corrosion Fatigue Crack Initiation," Met. Trans., 13A, 1982, p. 649.

18. Y. Kondo, "Prediction of Fatigue Crack Initiation Life Based on Pit Growth," Corrosion, 45, 1989, p. 7.

19. T. Kobayashi, SRI International, Menlo Park, CA (private communication).

20. Yoshiyuki Kondo and Robert P. Wei, "Approach On Quantitative Evaluation of Corrosion Fatigue Crack Initiation Condition," in International Conference on Evaluation of Materials Performance in Severe Environments, EVALMAT 89, Vol. 1, Kobe, Japan, November 20-23, 1989, The Iron and Steel Institute of Japan, Tokyo 100, Japan, 1989, pp. 135-142.

21. D. G. Harlow and R. P. Wei, "A Mechanistically Based Probability Approach for Predicting Corrosion and Corrosion Fatigue Life," in ICAF Durability and Structural Integrity of Airframes, Vol. I, A. F. Blom, ed., EMAS, Warley, United Kingdom, 1993, pp. 347-366.

22. D. Gary Harlow and Robert P. Wei, "Probability Approach for Corrosion and Corrosion Fatigue Life," J. of the Am. Inst. of Aeronautics and Astronautics, 32, 10, October, 1994, pp. 2073-2079.

23. D. Gary Harlow and Robert P. Wei, "Probability Modelling for the Growth of Corrosion Pits," 1995 ASME International Mechanical Engineering Congress and Exposition on Structural Integrity in Aging Aircraft, San Francisco, CA, 47, C. I. Chang and C. T. Sun, eds., The American Society of Mechanical Engineers, New York, NY 10017, 1995, pp. 185-194.

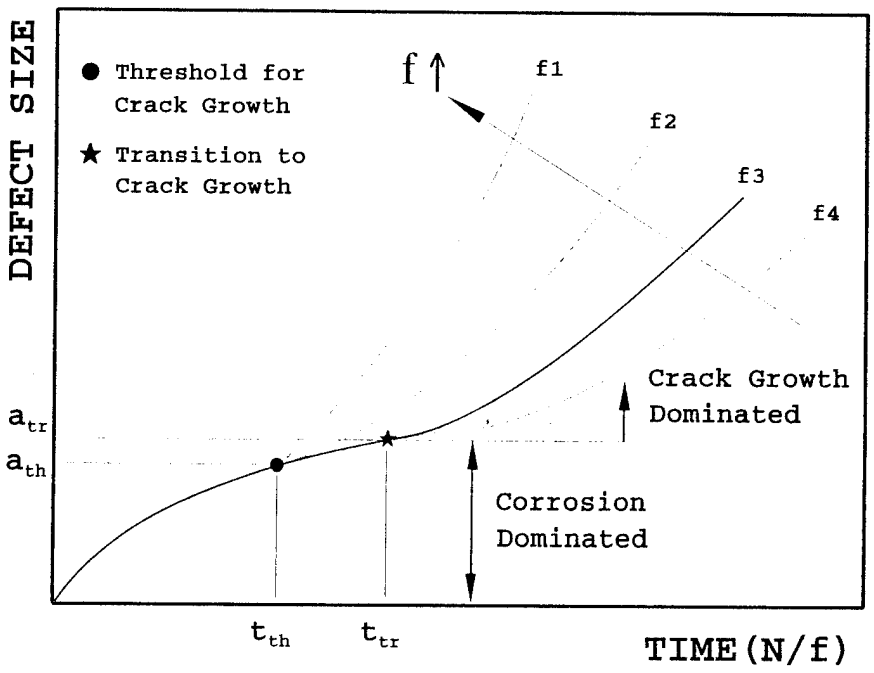

FIGURE 1. SCHEMATIC REPRESENTATION OF PITTING CORROSION AND CORROSION FATIGUE

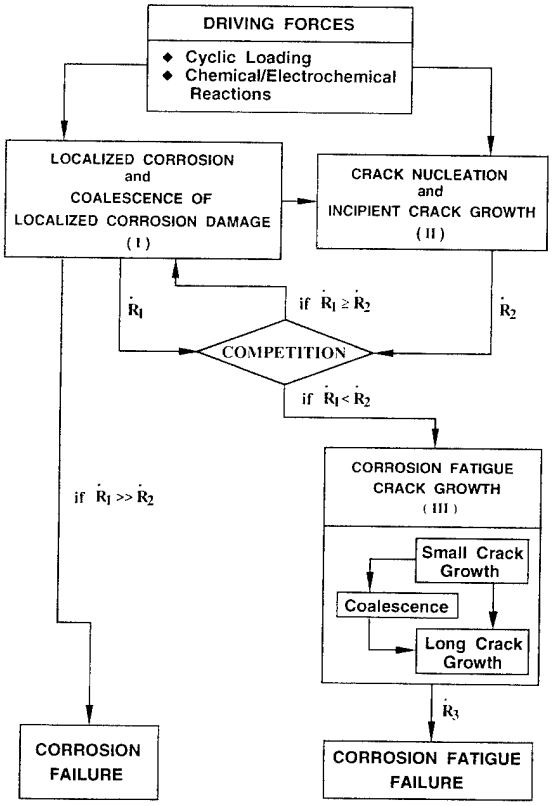

FIGURE 2. FLOW DIAGRAM SHOWING THE OVERALL PROCESSES FOR CORROSION AND FATIGUE DAMAGE

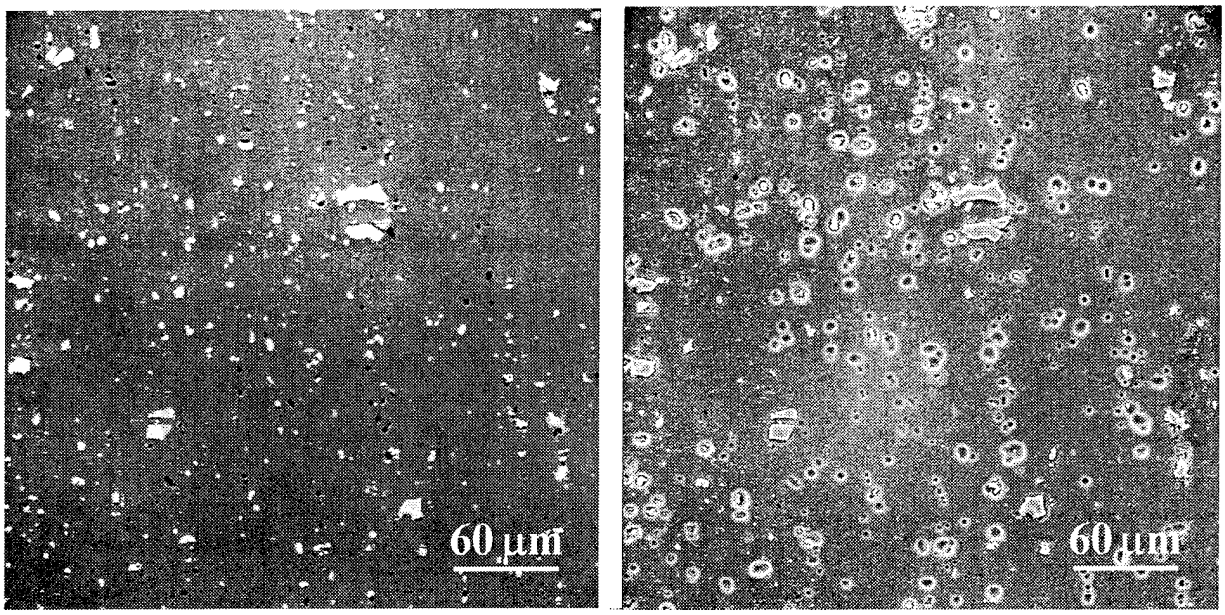

(a) (b)

FIGURE 3. SEM MICROGRAPHS SHOWING PARTICLES AND CORROSION PITS FOR THE SAME AREA OF (a) AS-POLISHED SURFACE (BACKSCATTERED ELECTRON IMAGES) BEFORE 3-DAY EXPOSURE, AND (b) CORRODED SURFACE (SECONDARY ELECTRON IMAGES) AFTER 3-DAY EXPOSURE TO 0.5 M NaCl SOLUTION AT ROOM TEMPERATURE

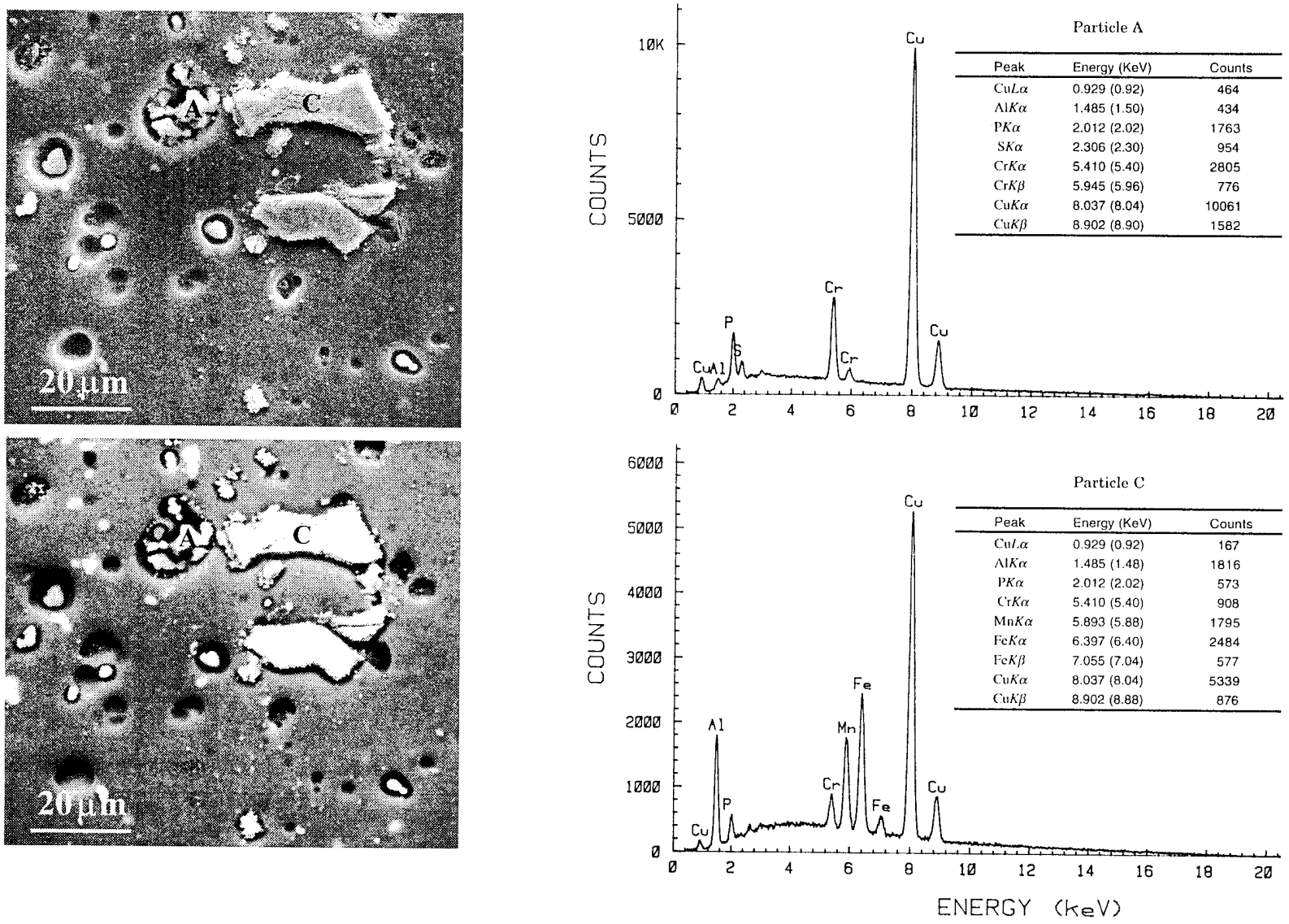

FIGURE 4. LOCALIZED CORROSION AT CONSTITUENT PARTICLES IN 2024-T3 ALUMINUM ALLOY SHOWING TYPE A AND TYPE C PARTICLES

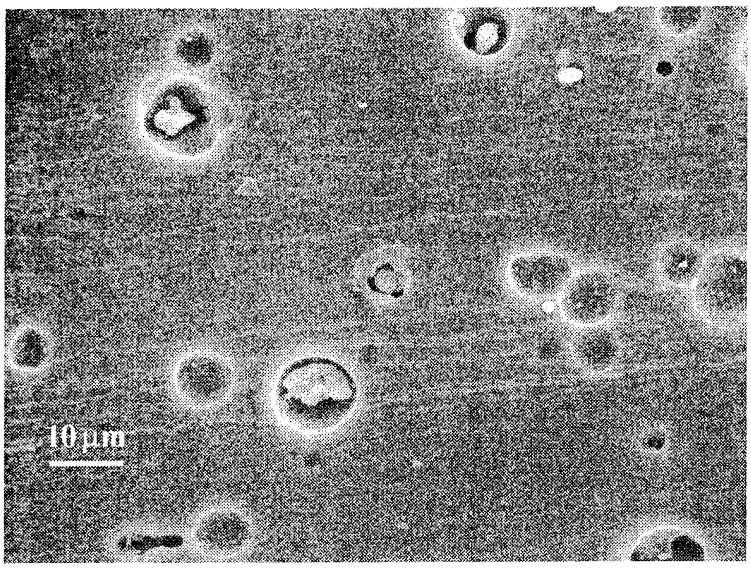

(a)

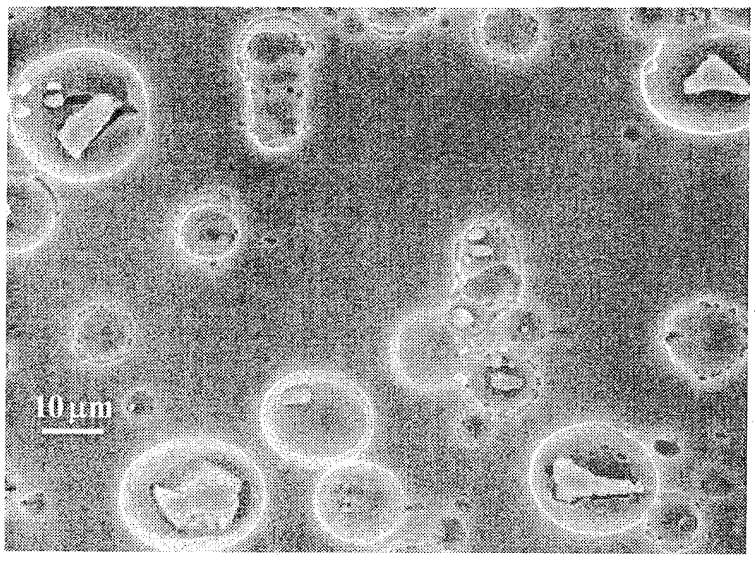

(b)

FIGURE 5. SCANNING ELECTRON MICROGRAPHS SHOWING PITTING ASSOCIATED WITH (a) TYPE A (*ANODIC*) PARTICLES, AND (b) TYPE C (*CATHODIC*) PARTICLES

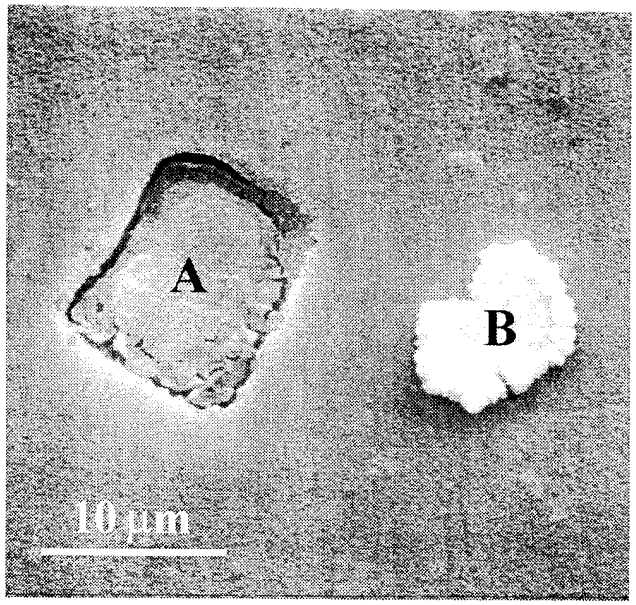

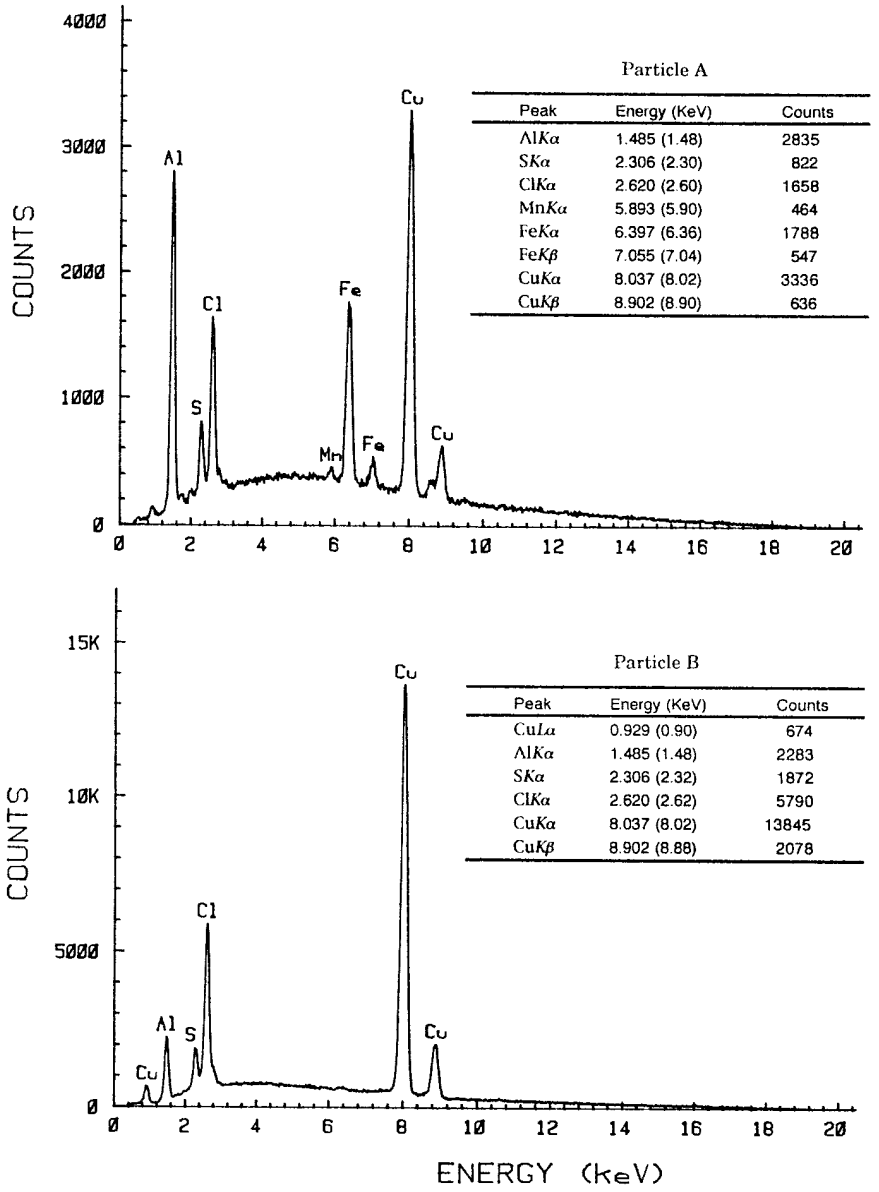

FIGURE 6. CORROSION FEATURES AND COMPOSITIONS OF TWO ADJACENT (DISSIMILAR) PARTICLES FOR A SPECIMEN TESTED AT 80°C FOR 3 HOURS

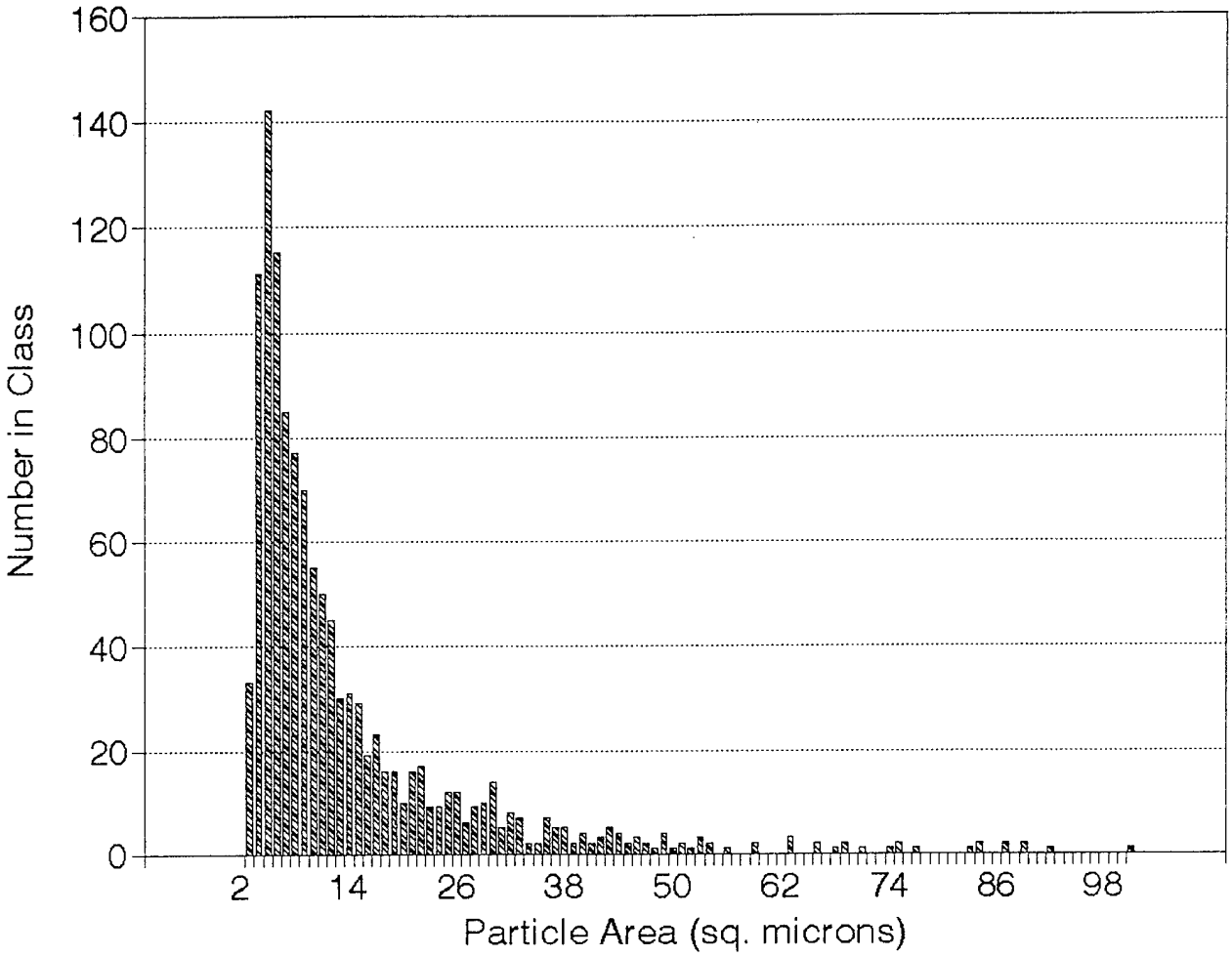

FIGURE 7. A HISTOGRAM OF THE SIZE DISTRIBUTION FOR CONSTITUENT PARTICLES ON THE SURFACE OF A 2024-T3 ALUMINUM SPECIMEN

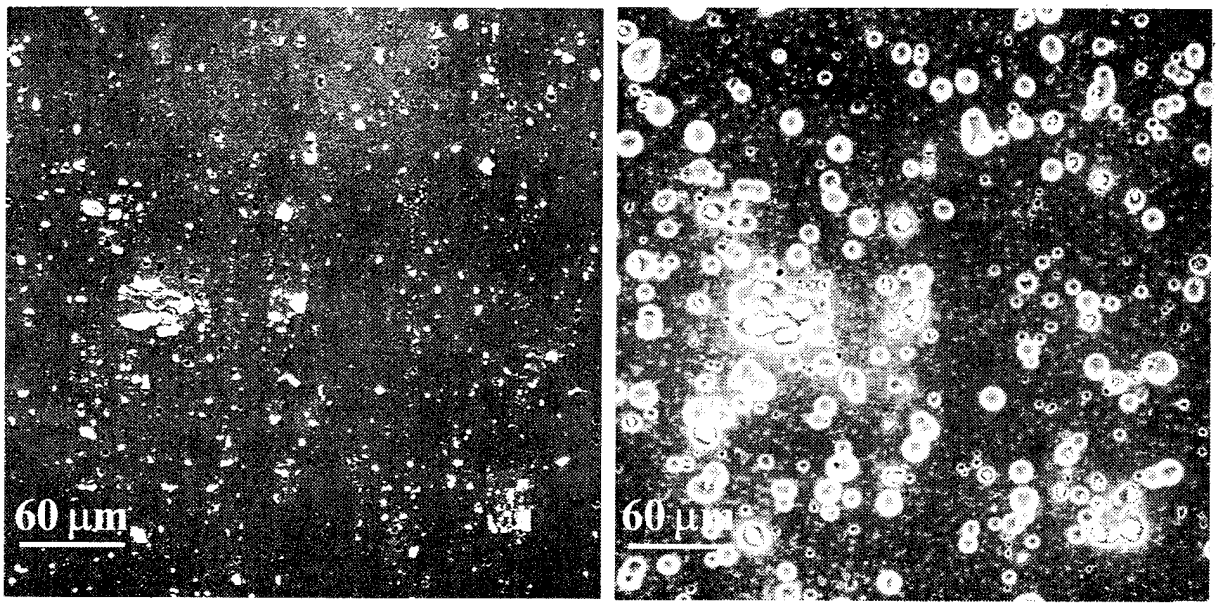

(a) (b)

FIGURE 8. SEM MICROGRAPHS SHOWING PARTICLES AND CORROSION PITS FOR THE SAME AREA OF (a) AS-POLISHED SURFACE (BACKSCATTERED ELECTRON IMAGES) BEFORE 3-DAY EXPOSURE, AND (b) CORRODED SURFACE (SECONDARY ELECTRON IMAGES) AFTER 3-DAY EXPOSURE TO 0.5M NaCl SOLUTION AT 65°C

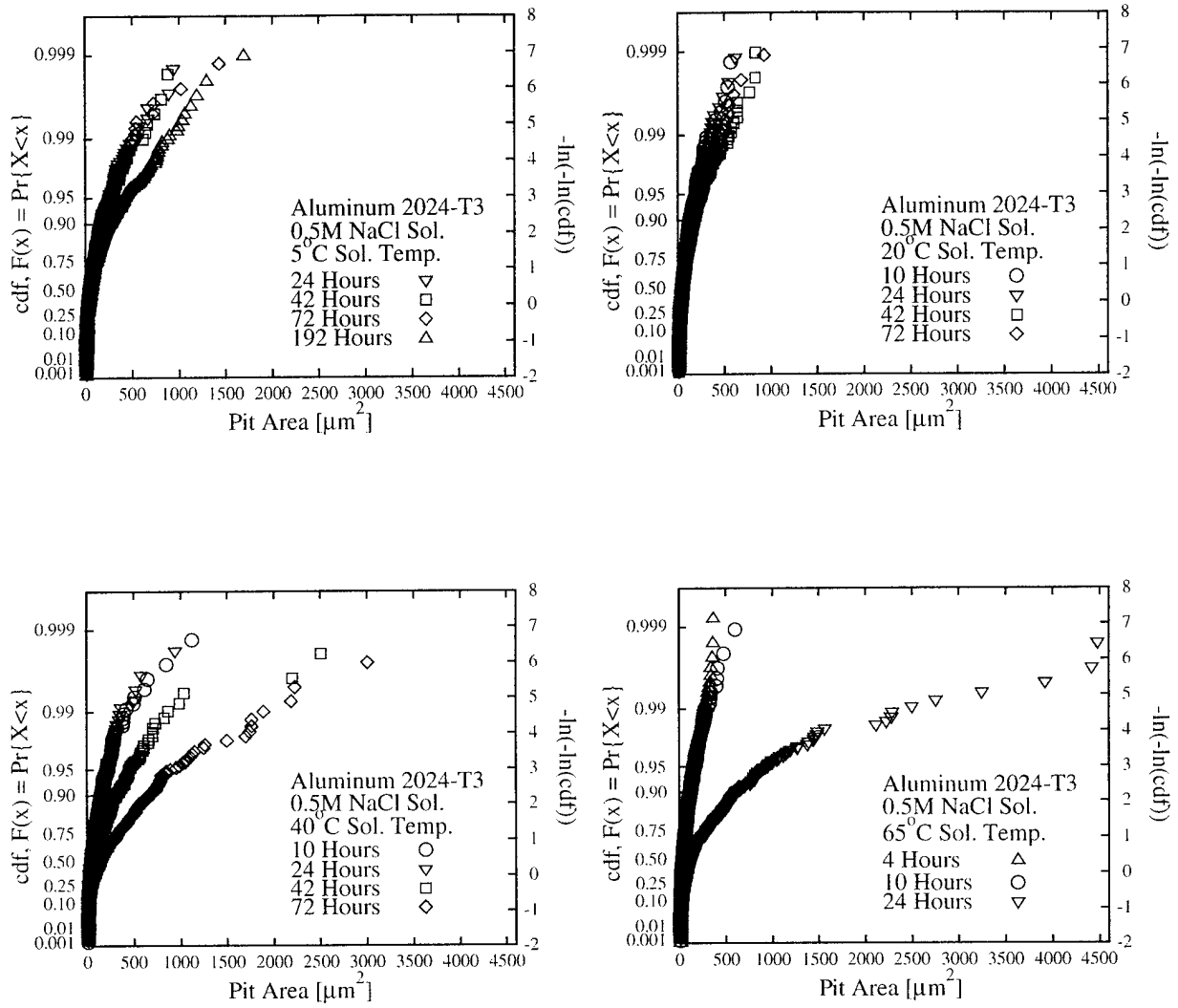

FIGURE 9. EXTREME VALUE (GUMBEL) PLOTS SHOWING EVOLUTION OF PIT SIZES AS A FUNCTION OF TIME AT 5, 20, 40 AND 65°C

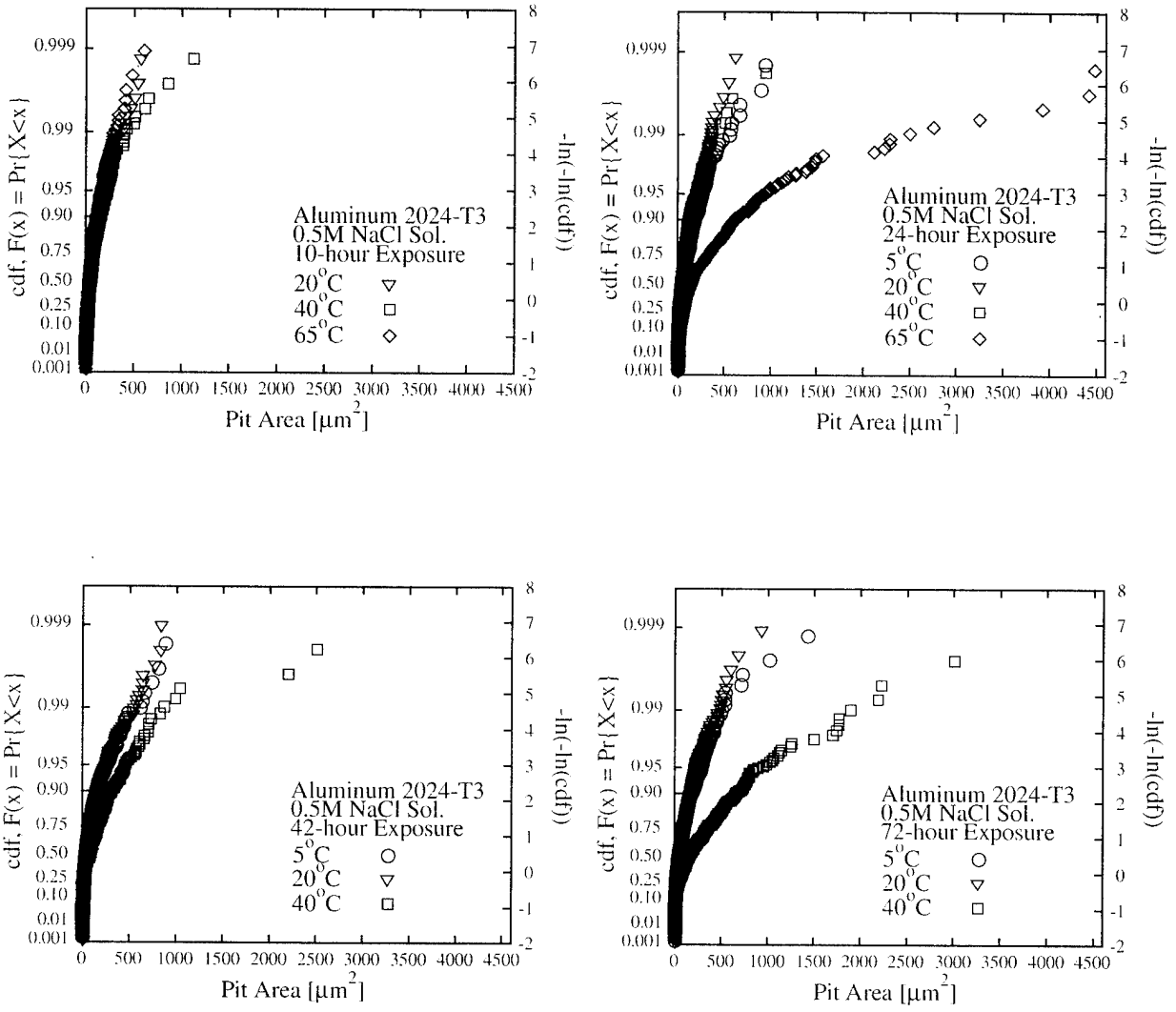

FIGURE 10. EXTREME VALUE (GUMBEL) PLOTS SHOWING EVOLUTION OF PIT SIZES AS A FUNCTION OF TEMPERATURE AT EXPOSURE TIMES OF 10, 24, 42 AND 72 HOURS

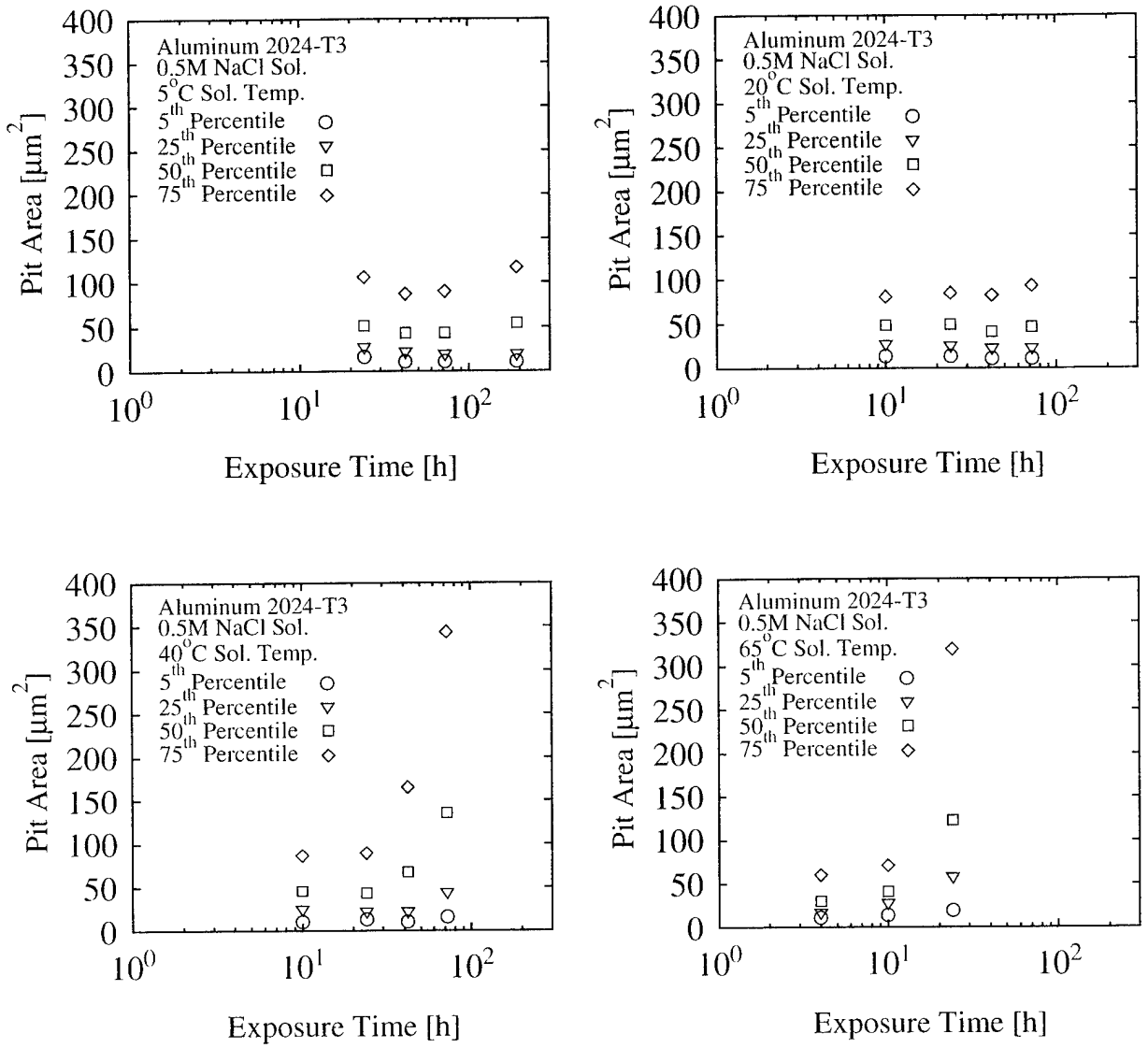

FIGURE 11. TIME EVOLUTION OF PIT SIZE AT SELECTED PROBABILITY (PERCENTILE) LEVELS

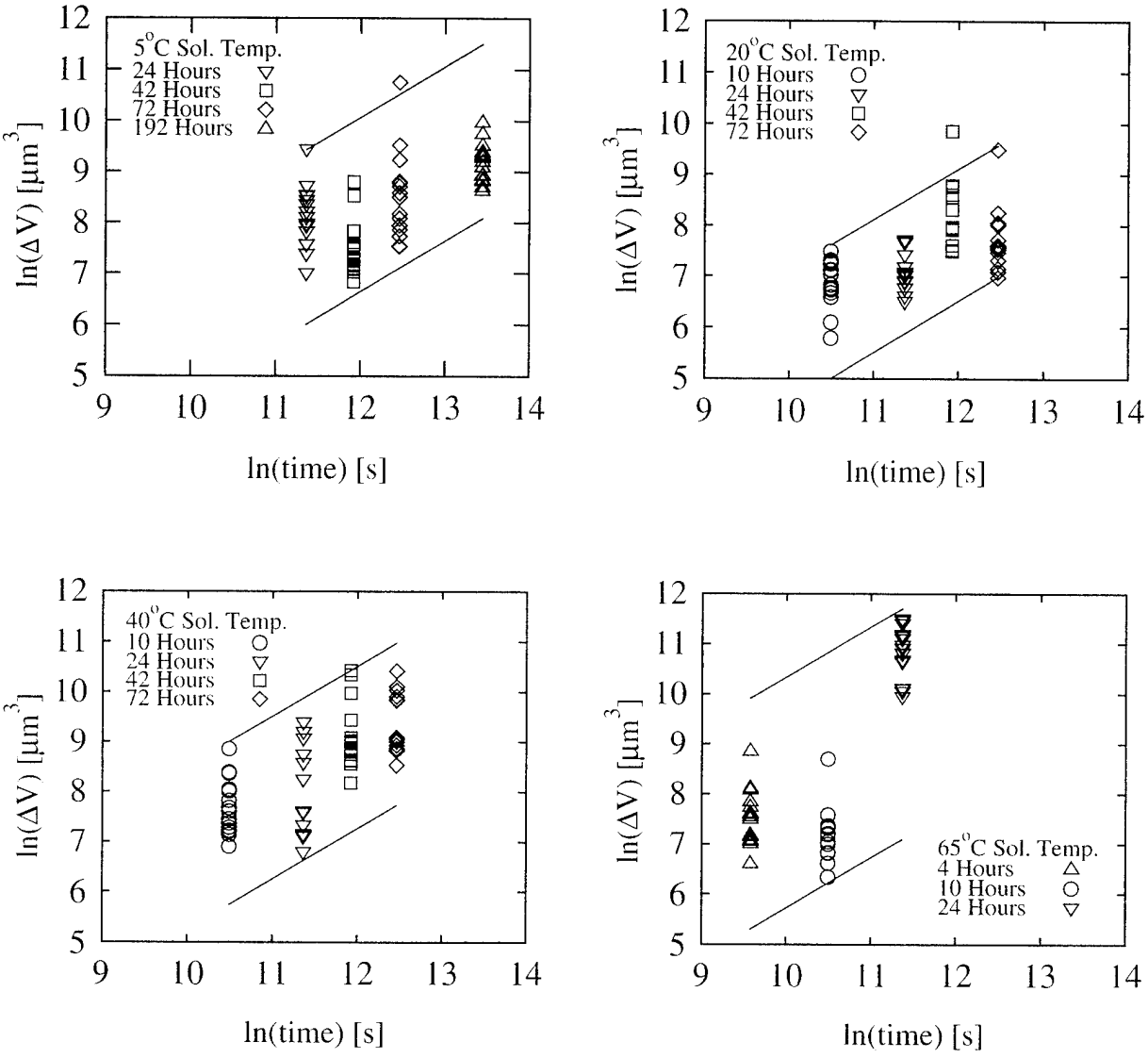

FIGURE 12. CHANGE IN PIT VOLUME VERSUS TIME (IN LOG-LOG COORDINATES) FOR THE FIFTEEN LARGEST PITS AT 5, 20, 40 AND 65°C. SOLID LINES INDICATE DATA TRENDS THAT REPRESENT A FARADAIC (CONSTANT VOLUME RATE) DISSOLUTION LAW

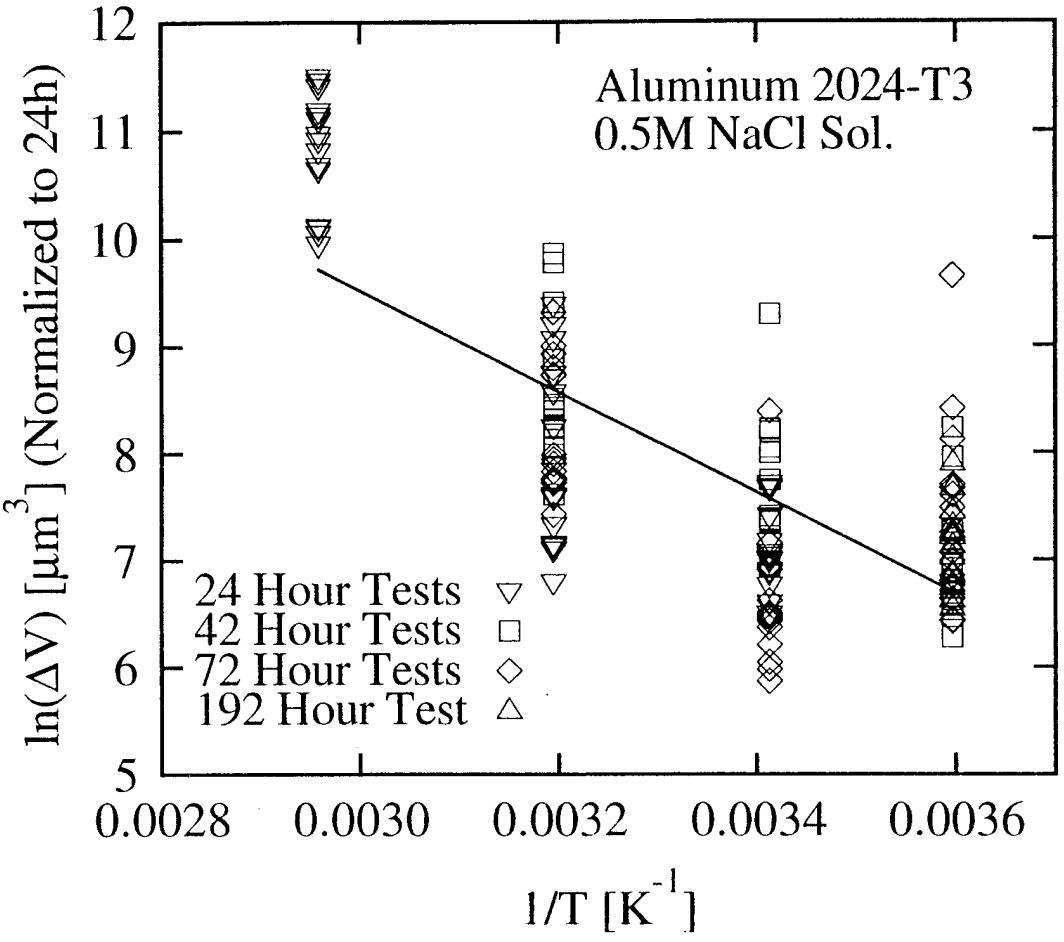

FIGURE 13. ARRHENIUS NORMALIZED PIT GROWTH DATA FROM FIGURE 12 SHOWING THERMALLY ACTIVATED CORROSION RESPONSE

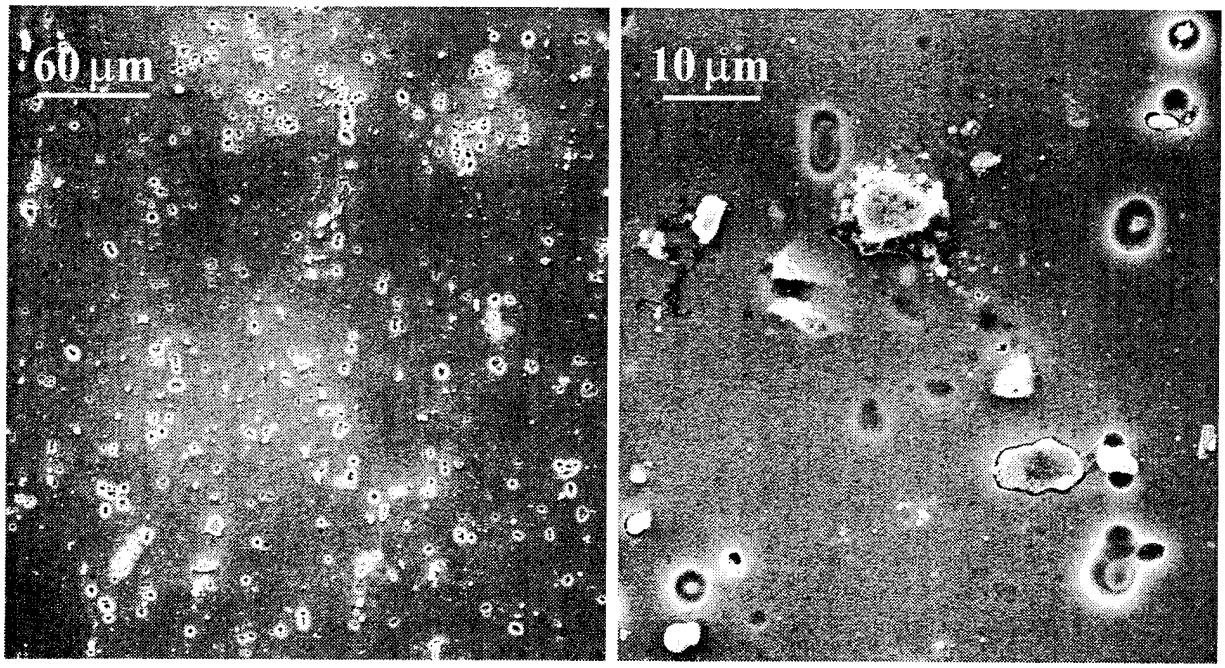

(a) (b)

FIGURE 14. CORRODED SURFACE MORPHOLOGIES A SPECIMEN EXPOSED TO 0.5M NaCl SOLUTION WITH pH = 3 FOR 3 DAYS AT ROOM TEMPERATURE: (a) 250X, AND (b) 1,300X.

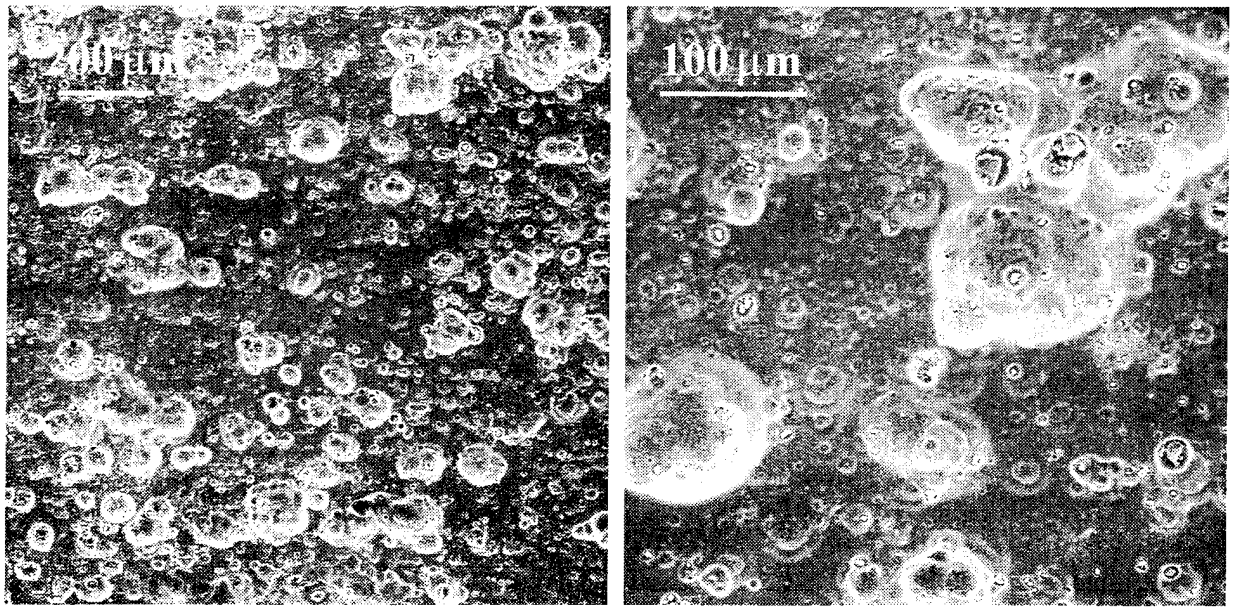

(a) (b)

FIGURE 15. CORRODED SURFACE MORPHOLOGIES FOR A SPECIMEN EXPOSED TO 0.5M NaCl SOLUTION WITH pH = 11 FOR 3 DAYS AT ROOM TEMPERATURE: (a) 65X, AND (b) 200X

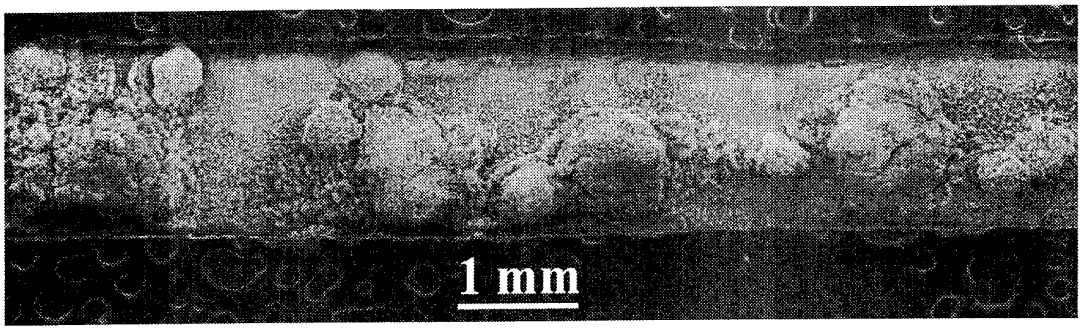

(a) As corroded

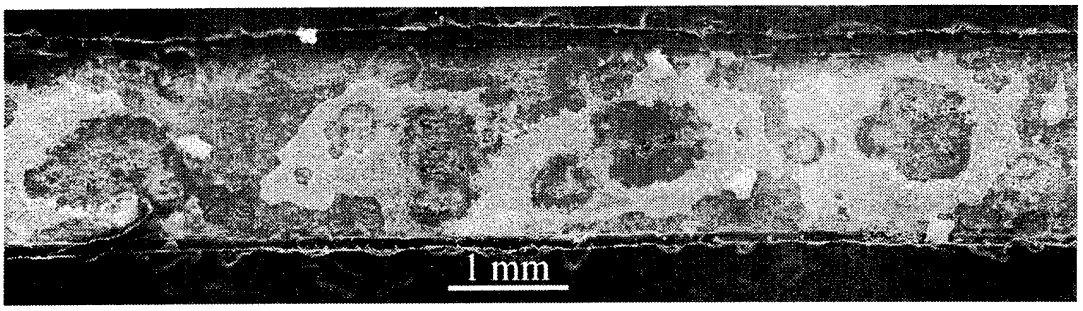

(b) After cleaning

FIGURE 16. OPTICAL MICROGRAPH OF THE CORRODED 2024-T3 ALLOY (LS) SURFACE (a) BEFORE, AND (b) AFTER "CLEANING" BY DRY STRIPPING

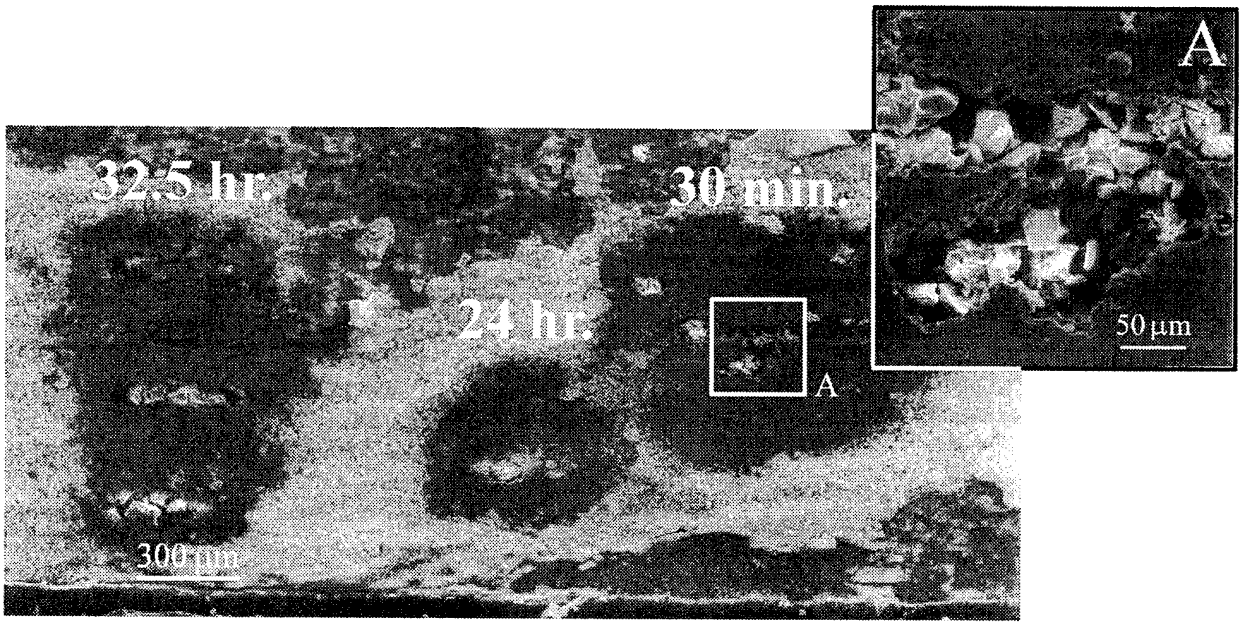

FIGURE 17. SEM MICROGRAPH OF LOCALIZED SEVERE PITS SHOWING CLUSTERS OF CONSTITUENT PARTICLES WITHIN THE PITS AND OTHER LOCAL DAMAGE (SEE INSET) IN THE 2024-T3 ALLOY.

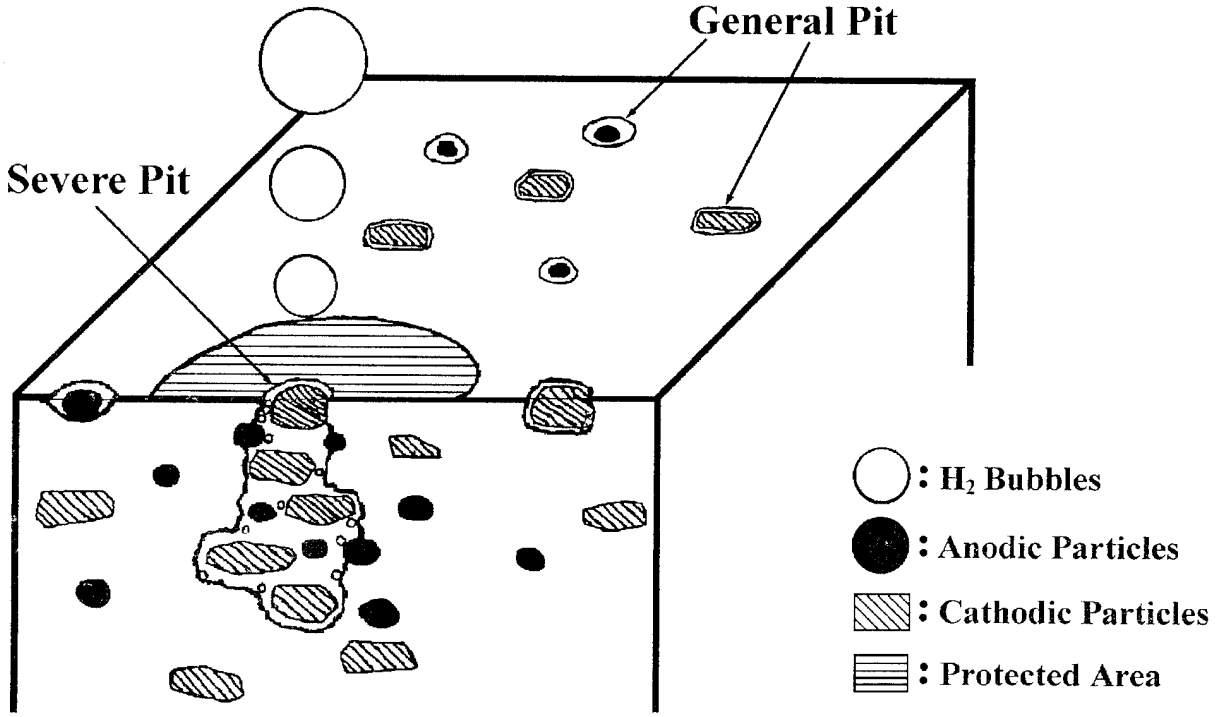

FIGURE 18. SCHEMATIC DIAGRAM OF A CONCEPTUAL MODEL FOR PITTING IN THE TRANSVERSE ORIENTATION INVOLVING MATRIX DISSOLUTION AROUND CLUSTERS OF CATHODIC (TYPE C) CONSTITUENT PARTICLES

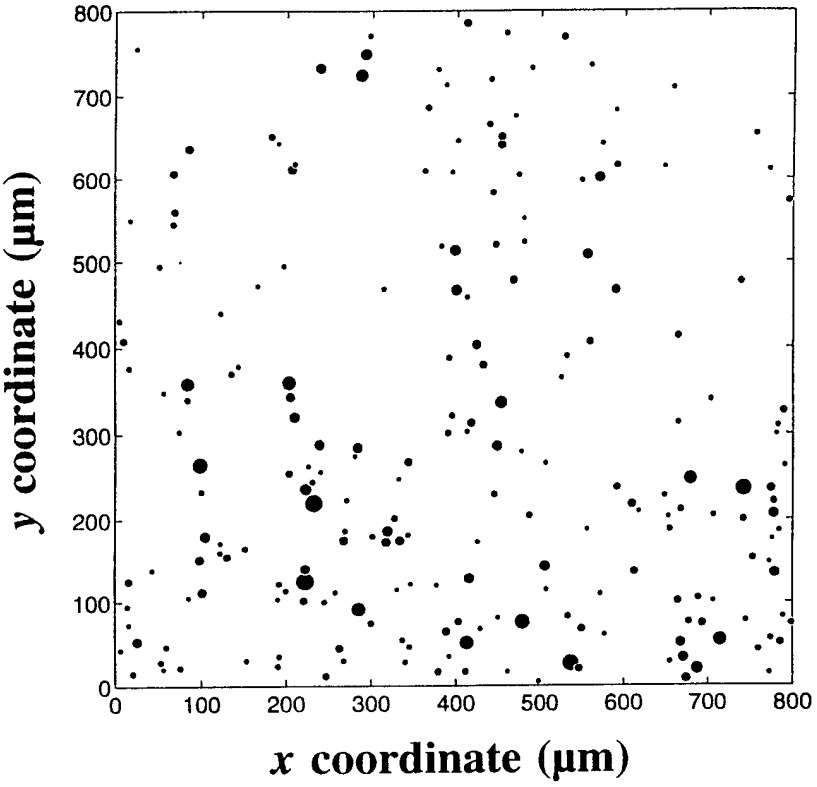

FIGURE 19. LOCATIONS AND EQUIVALENT AREAS OF PARTICLES IN THE ROLLING (LT) PLANE OF A 2024-T3 ALUMINUM ALLOY PRIOR TO CORROSION (*cf*, FIGURE 18).

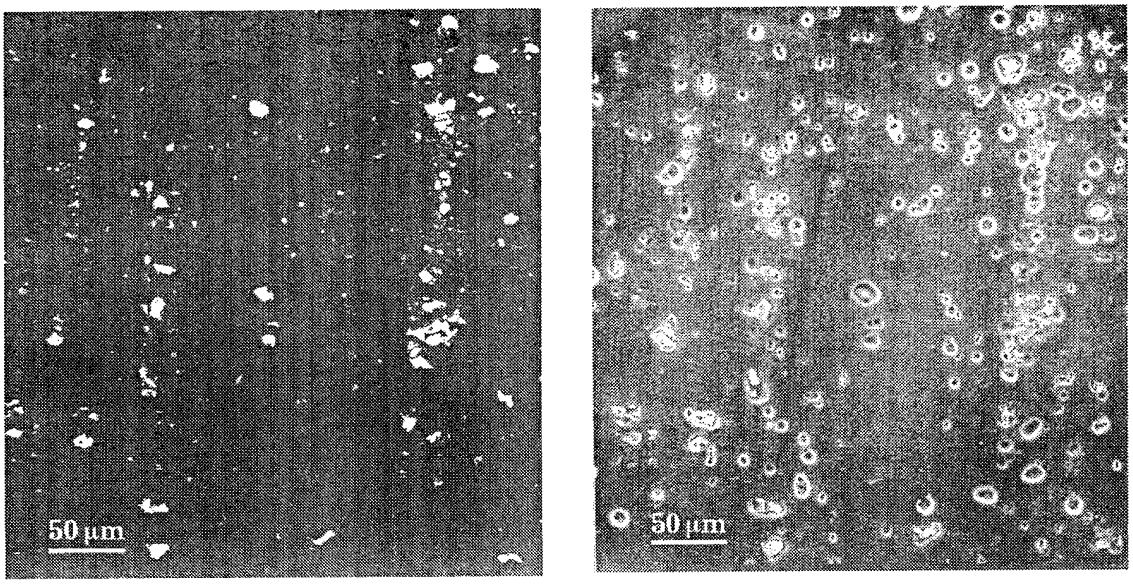

(a) Before (b) After

FIGURE 20. A COMPARISON OF ROLLING (LT) SURFACES OF A 2024-T3 ALUMINUM ALLOY BEFORE AND AFTER CORROSION (@ 40°C)

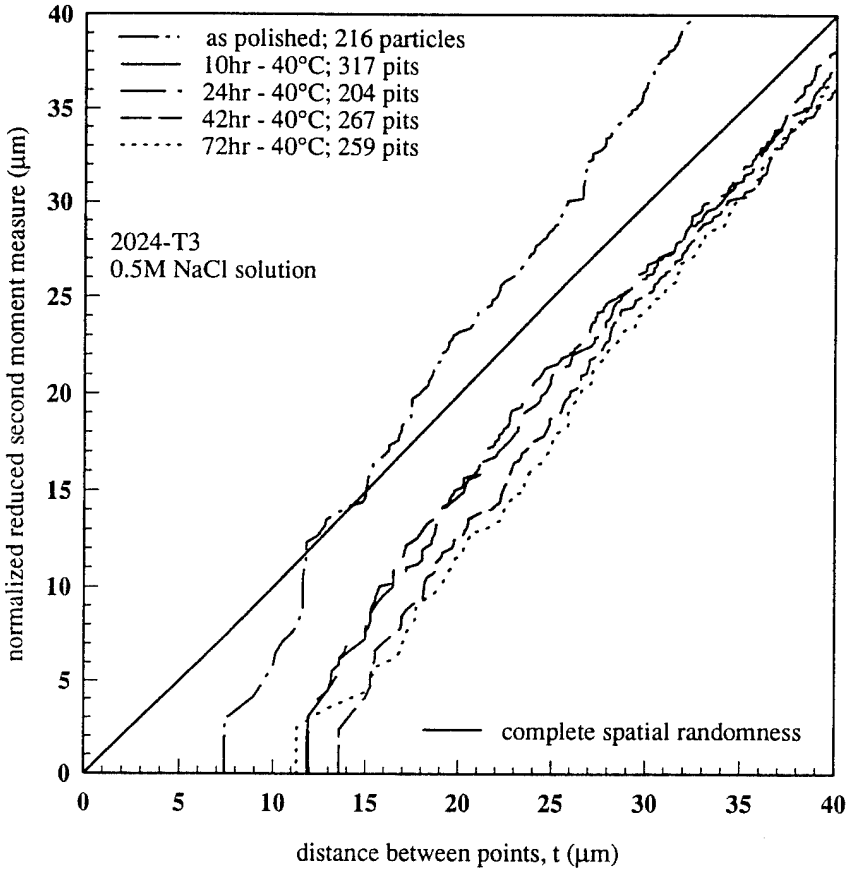

FIGURE 21. PLOT OF SECOND ORDER PROPERTIES FOR THE DISTRIBUTION OF PARTICLES/PITS IN A 2024-T3 ALUMINUM ALLOY.

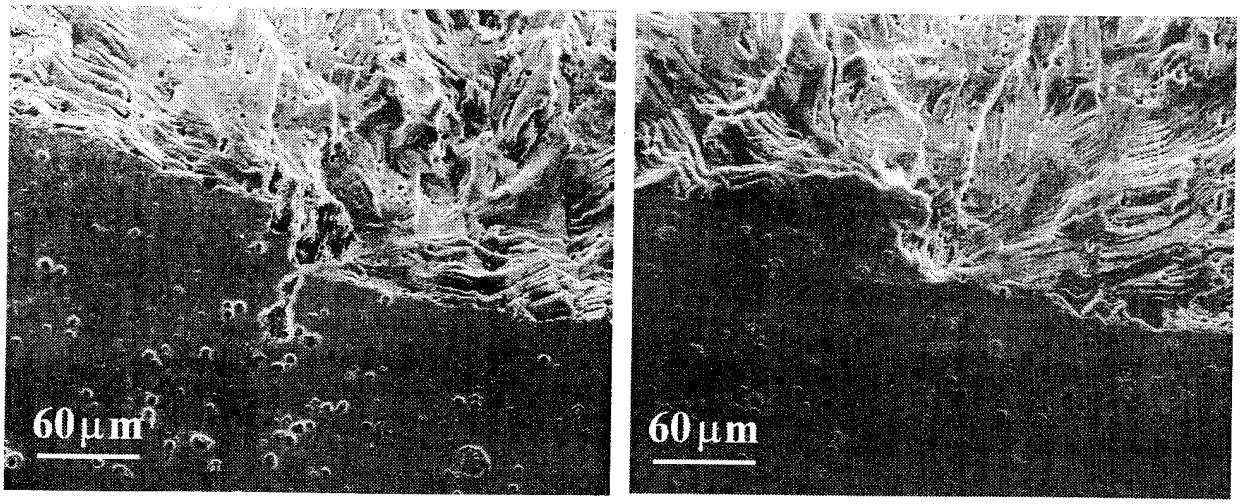

FIGURE 22. MATING SURFACES SHOWING INITIATION AND EARLY GROWTH OF FATIGUE CRACK FROM LOCALIZED CORROSION DAMAGE IN AN OPEN-HOLE SPECIMEN OF 2024-T3 ALUMINUM ALLOY AT 10 Hz $(\sigma_{max})_{hole}$ =320 MPa, R = 0.1)

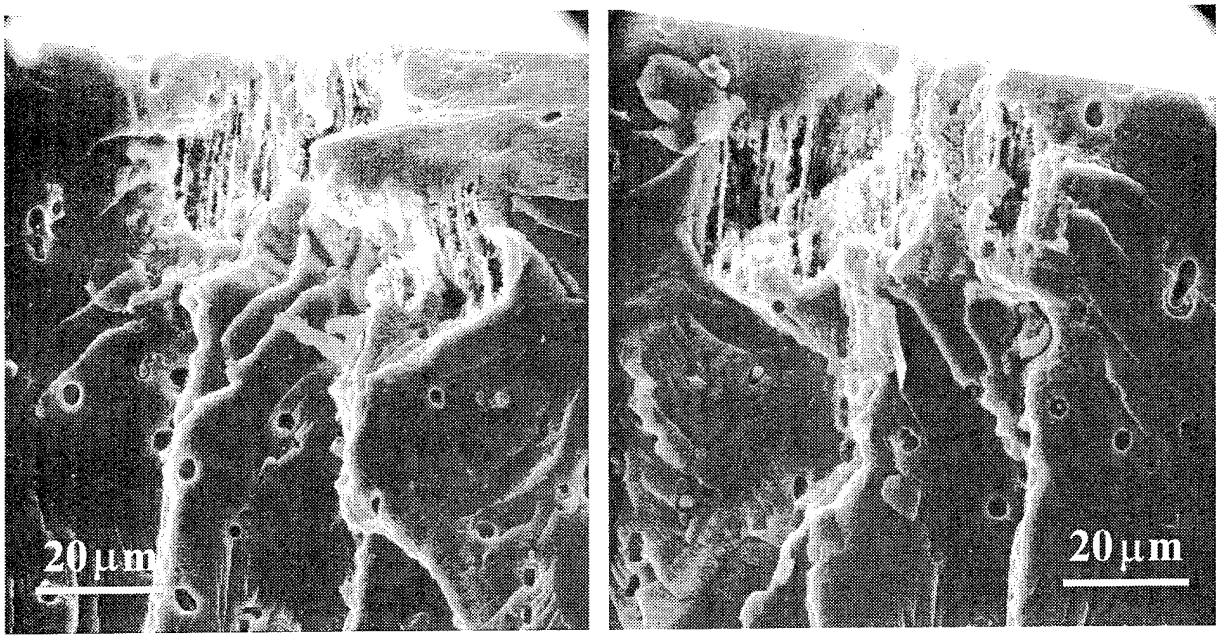

FIGURE 23. EXTENSIVE SUBSURFACE CORROSION DAMAGE AT THE NUCLEATION SITE (MATCHING SURFACES) IN SPECIMEN SHOWN IN FIGURE 22.

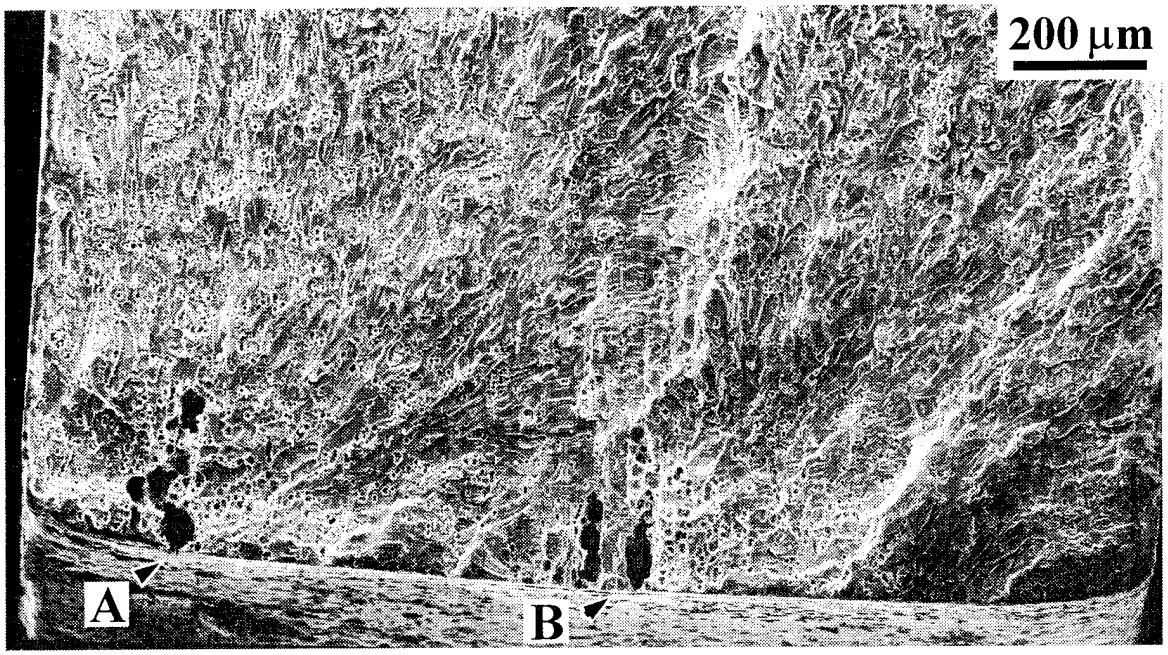

FIGURE 24. MATING SURFACES SHOWING INITIATION AND EARLY GROWTH OF FATIGUE CRACK FROM LOCALIZED CORROSION DAMAGE IN AN OPEN-HOLE SPECIMEN OF 2024-T3 ALUMINUM ALLOY AT 0.1 Hz $(\sigma_{max})_{hole}$ =320 MPa, R = 0.1)

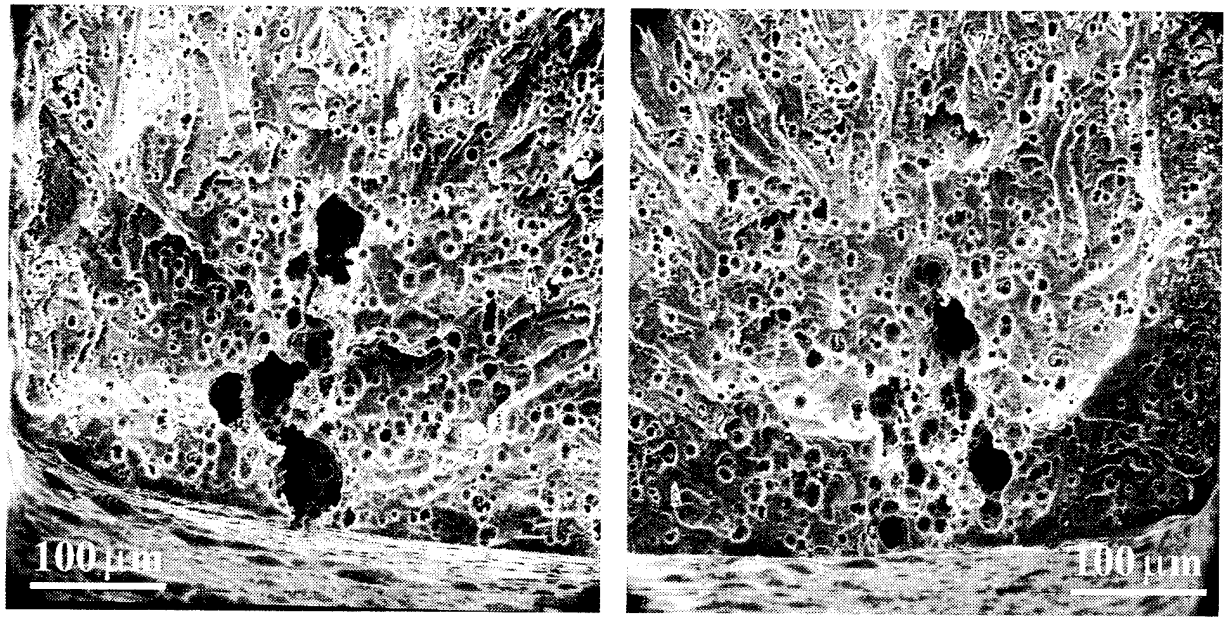

FIGURE 25. MATING SURFACES SHOWING INITIATION SITE A IN FIGURE 24 (NOTE PITTING OF THE FATIGUE FRACTURE SURFACES).

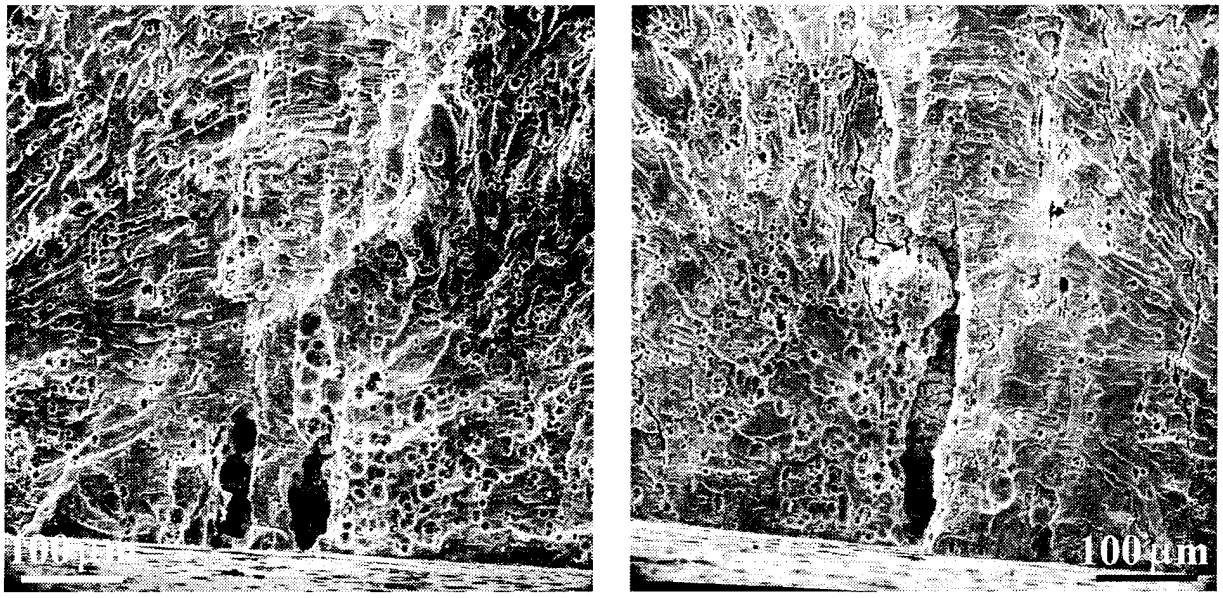

FIGURE 26. MATING SURFACES SHOWING INITIATION SITE B IN FIGURE 24 (NOTE PITTING OF THE FATIGUE FRACTURE SURFACES)

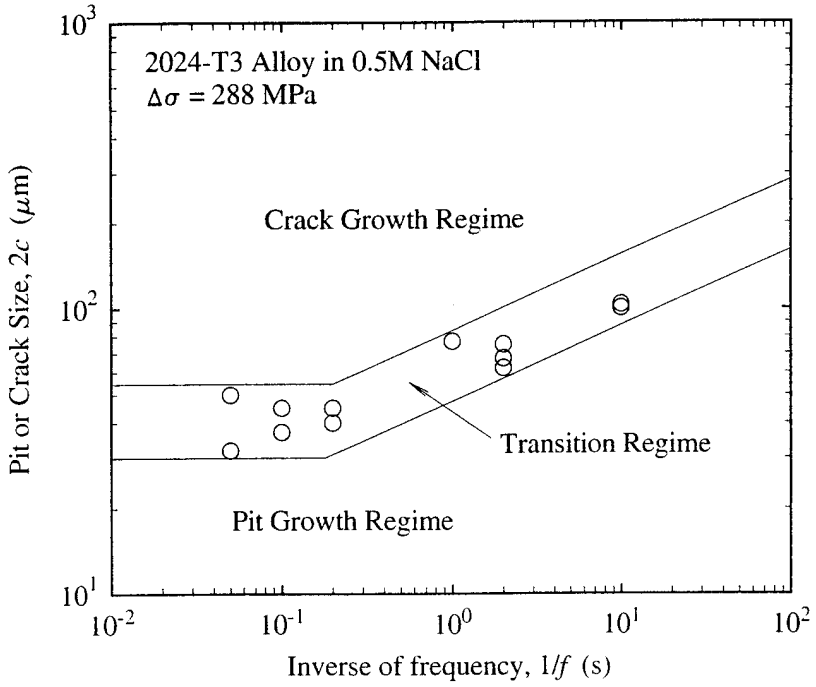

FIGURE 27. THE RELATIONSHIP BETWEEN THE PIT SIZE AT FATIGUE CRACK NUCLEATION AND THE INVERSE OF LOADING FREQUENCY.

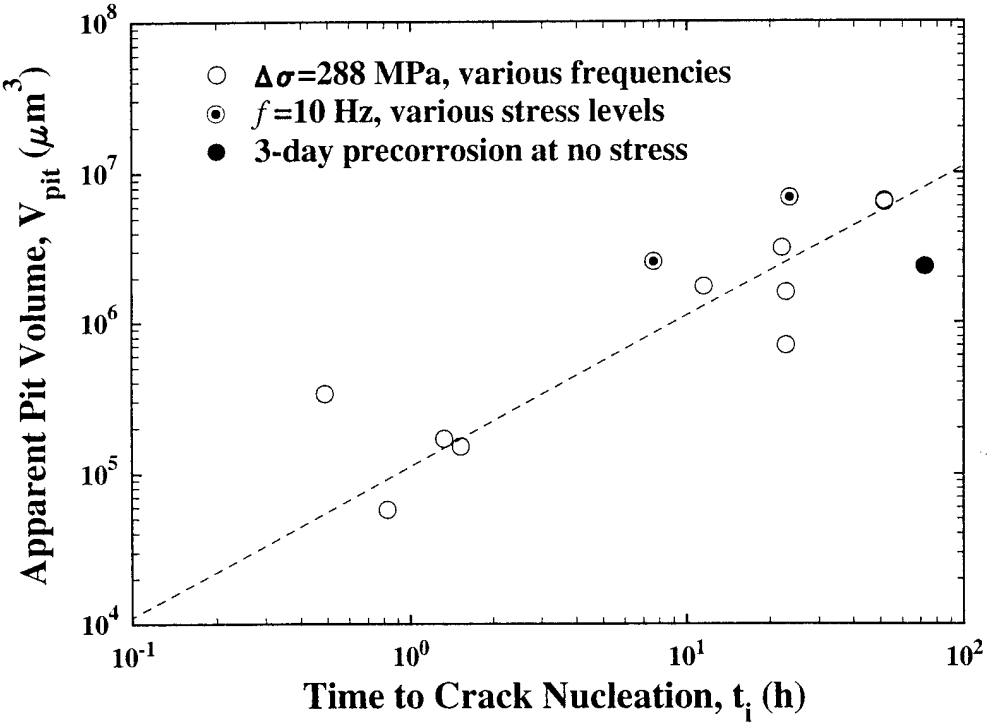

FIGURE 28. THE DEPENDENCE OF TRANSITION PIT SIZE ON EXPOSURE TIME IN 0.5M NaCl SOLUTION AT ROOM TEMPERATURE

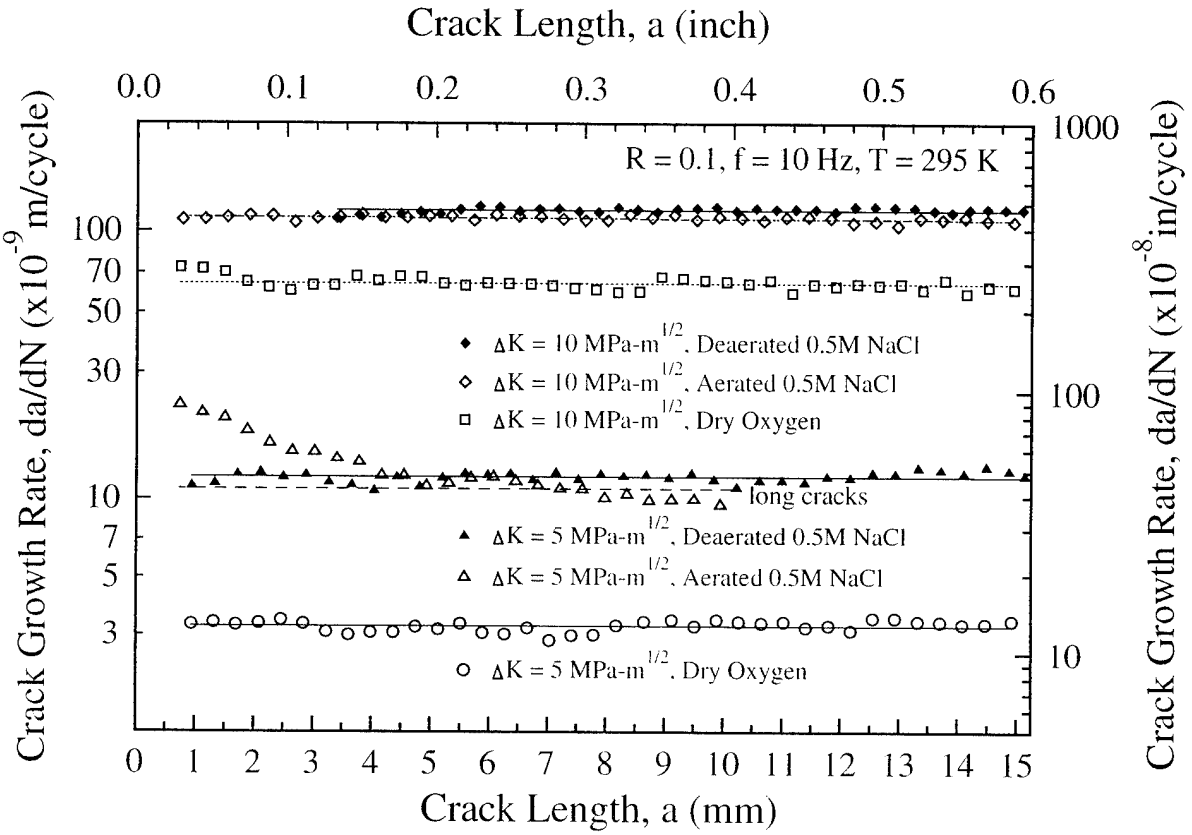

FIGURE 29. CORROSION FATIGUE CRACK GROWTH RATE AS A FUNCTION OF CRACK LENGTH SHOWING THE EFFECTS OF ΔK AND ENVIRONMENT AT ROOM TEMPERATURE

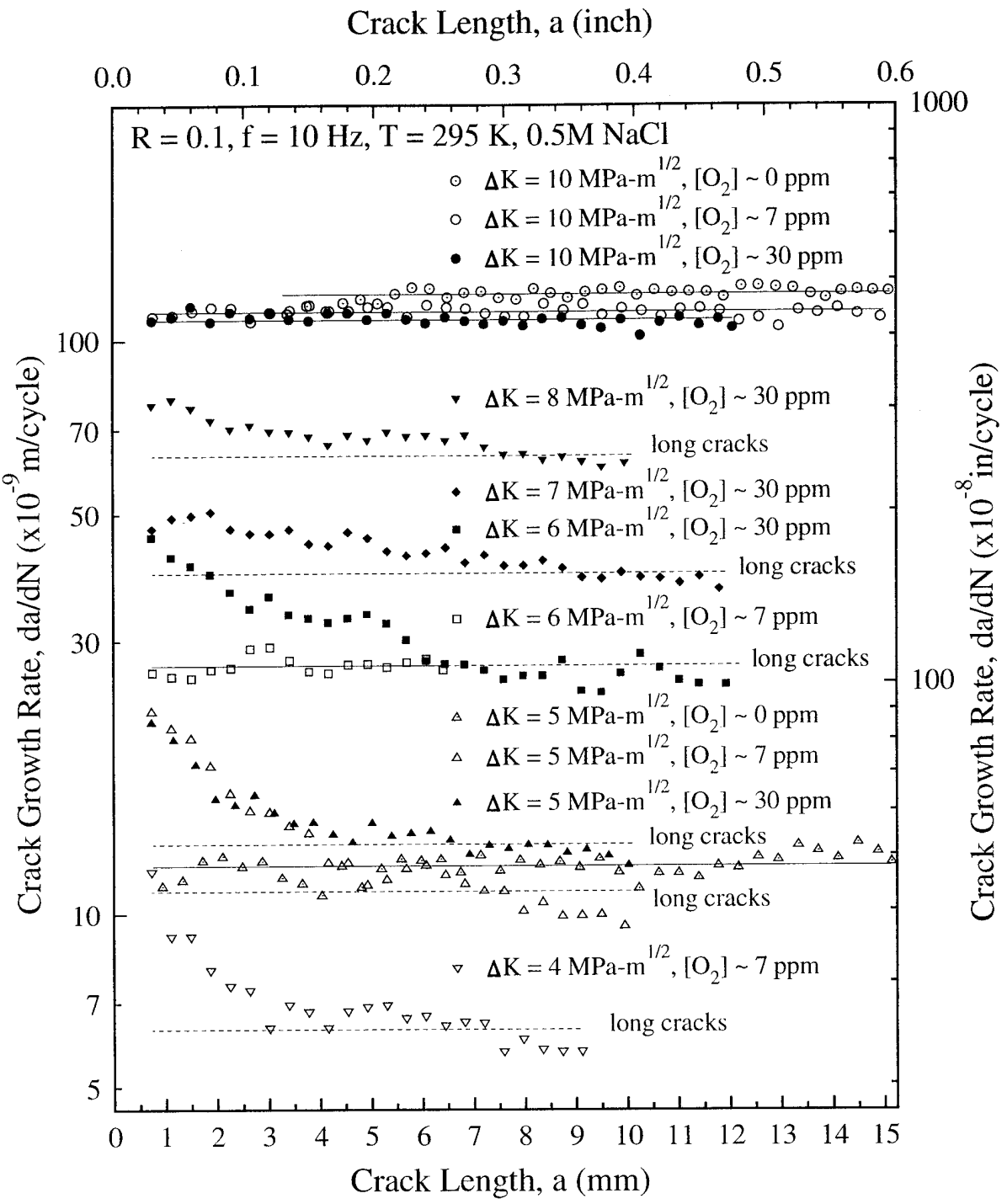

FIGURE 30. EFFECTS OF ΔK LEVEL AND OXYGEN CONCENTRATION ON CHEMICALLY SHORT CRACKS

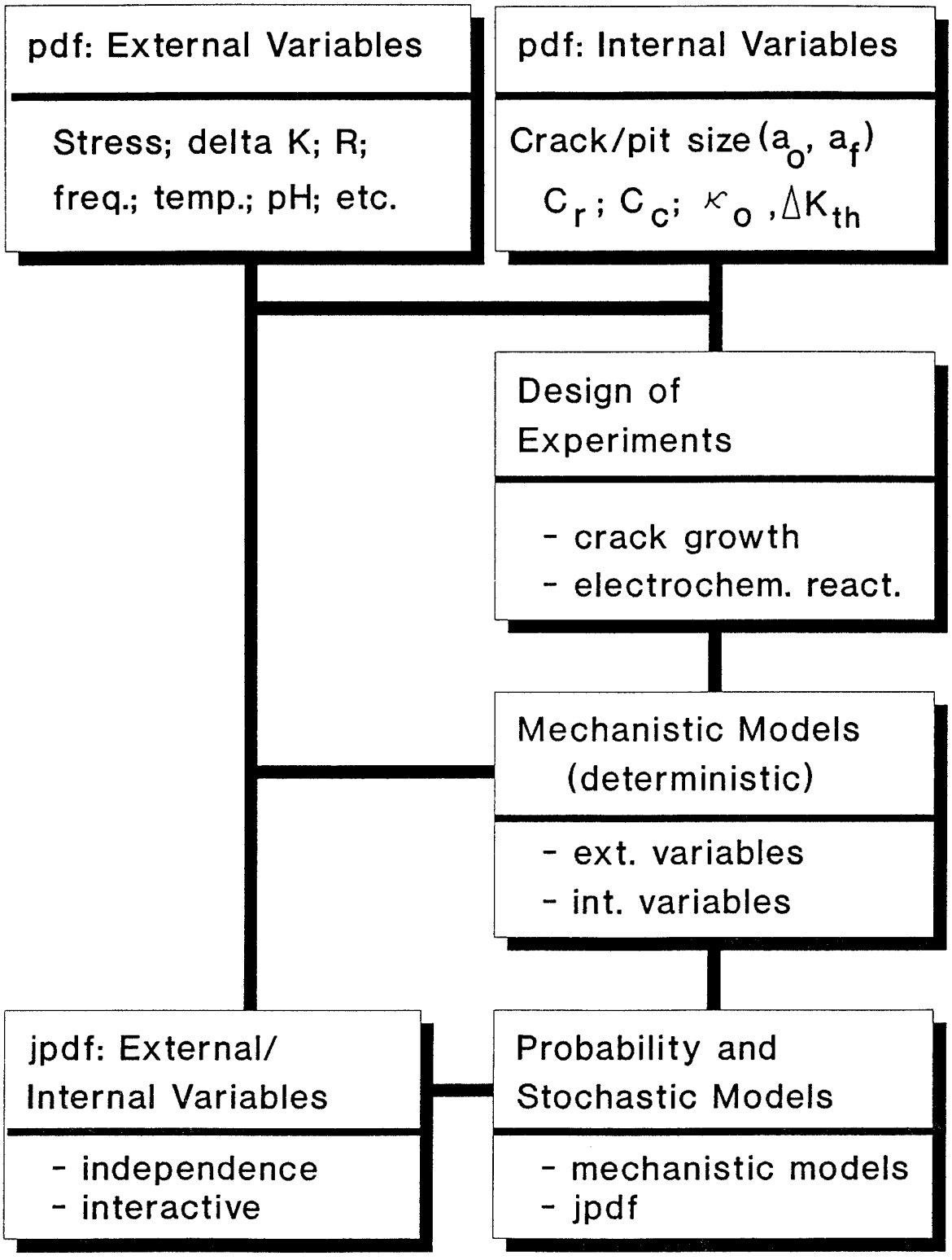

FIGURE 31. KEY ELEMENTS FOR THE FORMULATION OF A MECHANISTICALLY BASED PROBABILITY MODEL FOR LIFE PREDICTION

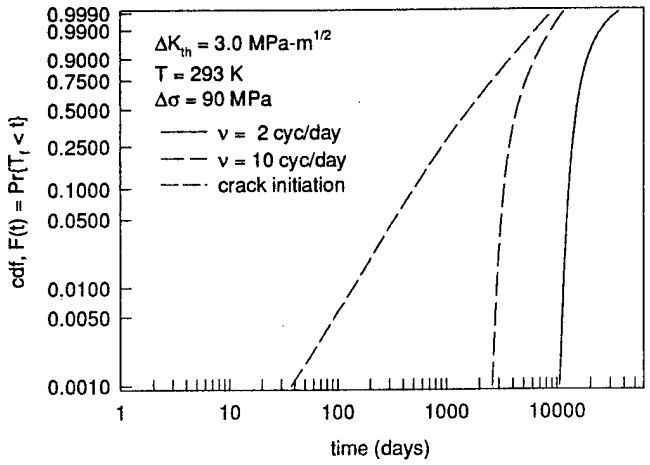

(a)

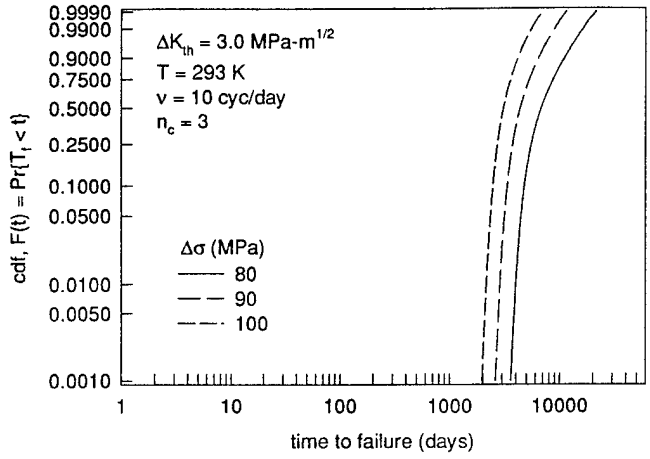

(b)

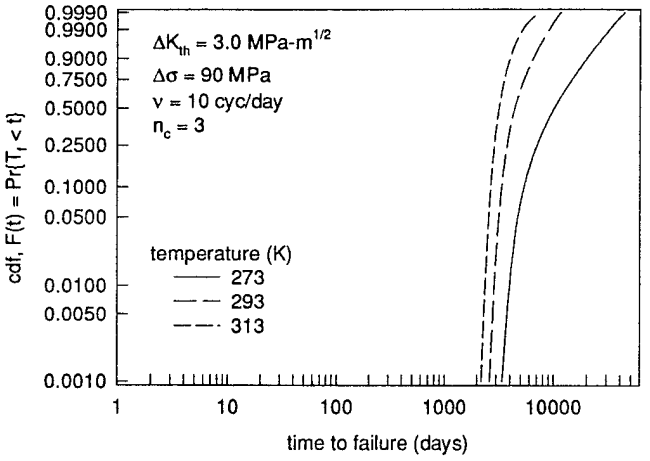

(c)

FIGURE 32. TYPICAL RESULTS SHOWING THE INFLUENCES OF LOADING (a) FREQUENCY, (b) APPLIED STRESS, AND (c) TEMPERATURE FOR PITTING CORROSION AND FATIGUE CRACK GROWTH FROM AN OPEN-HOLE SPECIMEN

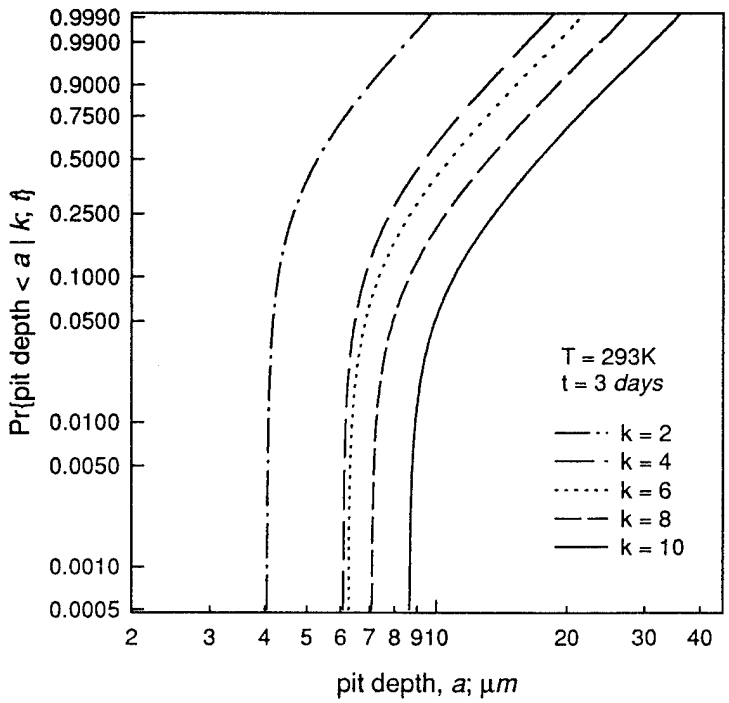

FIGURE 33. CONDITIONAL *CDFs* FOR PIT DEPTH WHEN THE NUMBER OF PARTICLES PER CLUSTER, *k*, IS 2, 4, 6, 8 AND 10, GIVEN AN EXPOSURE TIME OF 3 *DAYS* TO THE ENVIRONMENT AT A TEMPERATURE OF 293 K

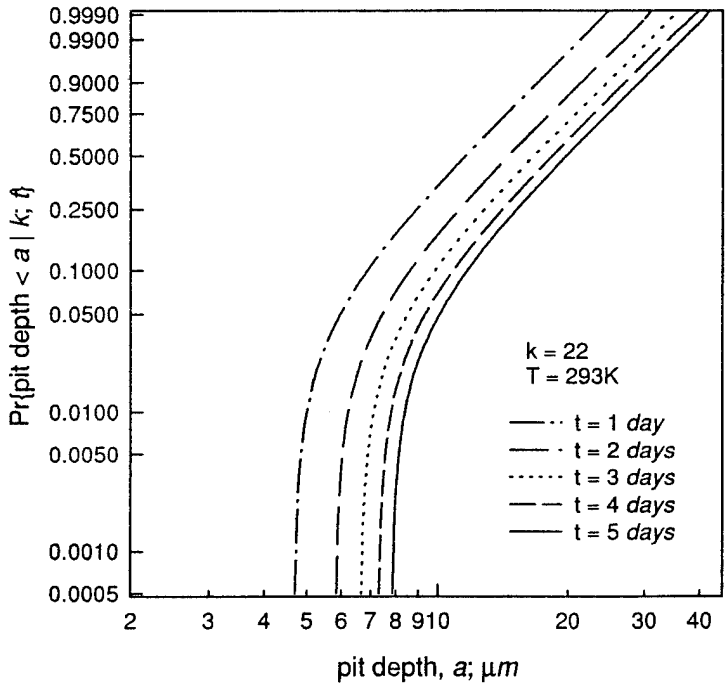

FIGURE 34. CONDITIONAL *CDFs* FOR PIT DEPTH WHEN THE EXPOSURE TIME, *t*, IS 1, 2, 3, 4 and 5 *DAYS*, GIVEN 22 PARTICLES PER CLUSTER AND A TEMPERATURE OF 293 K

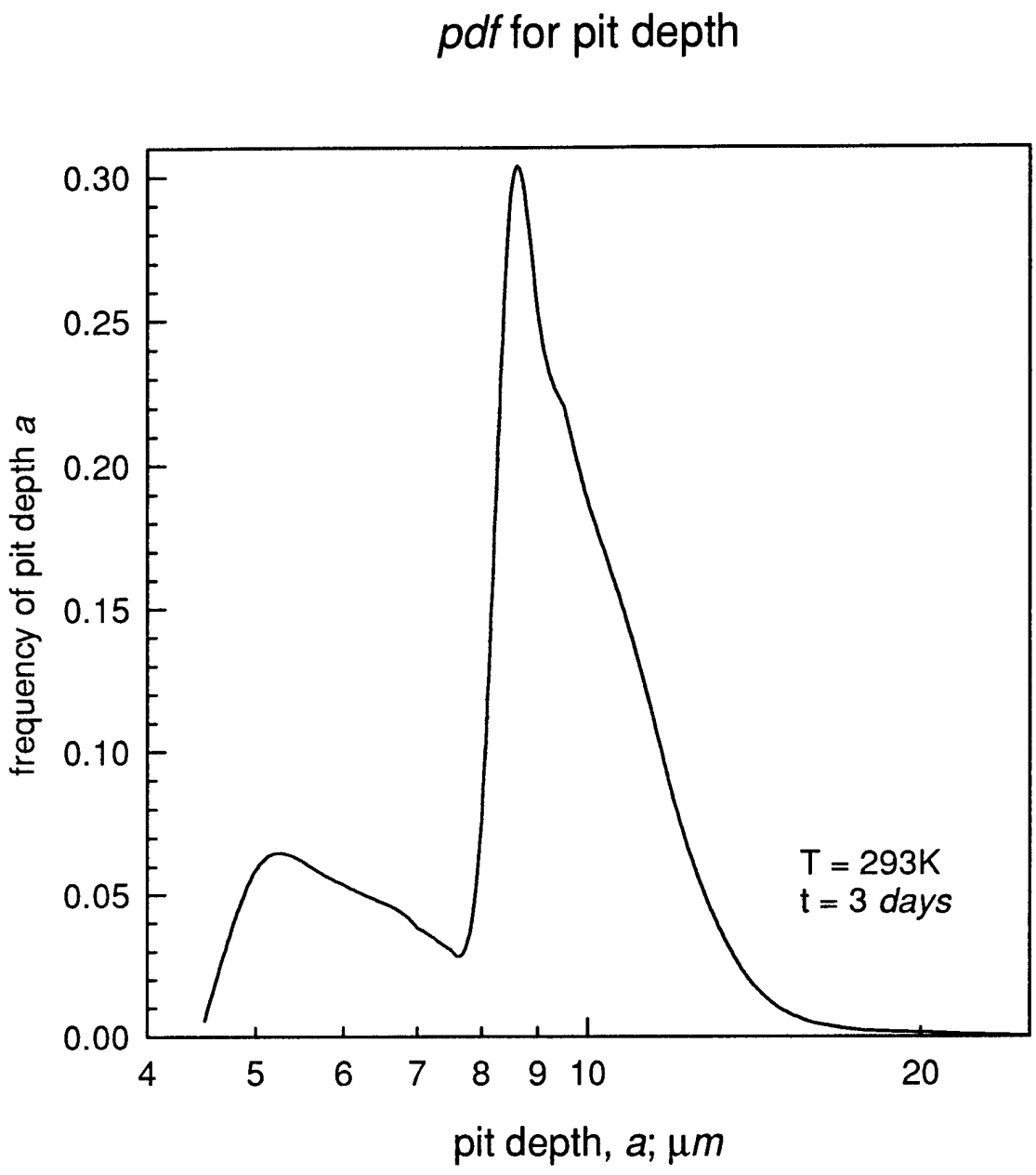

FIGURE 35. THE *pdf* FOR PIT DEPTH FOLLOWING 3 DAYS OF EXPOSURE AT ROOM TEMPERATURE

TABLE 1: COMPARISON OF EDX RESULTS FOR INDIVIDUAL PARTICLES BEFORE AND AFTER CORROSION IN 0.5M NaCl SOLUTION AT 80°C FOR 24 HOURS

Particle Type	Corrosion Testing	*Ka* Intensity (counts)				
		Mg	Mn	Fe	Cu	Al
A1	before	678	ND	ND	9600	2990
	after	ND	ND	495	11362	474
A2	before	804	ND	ND	7086	3516
	after	ND	523	640	5710	1892
A3	before	1437	ND	ND	6593	8411
	after	ND	468	534	6354	840
A4	before	2209	ND	ND	2798	11024
	after	ND	681	619	5061	4671
C1	before	ND	3485	4644	4379	1057
	after	ND	433	1092	9666	4671
C2	before	ND	2132	2972	5541	2086
	after	ND	702	3078	7843	700
C3	before	ND	3280	3960	4067	5057
	after	ND	968	5072	3359	1337
C4	before	ND	2723	3438	4725	5997
	after	ND	689	4997	2443	1470

ND: not detected

TABLE 2: ELEMENTAL COMPOSITION OF CONSTITUENT PARTICLES (ATOMIC PERCENT)

Type/Element	Al	Cu	Mg	Fe	Mn
TYPE A	52.8±0.8	24.5±0.4	22.7±0.5	--	--
TYPE C	76.6±0.4	7.8±0.9	--	8.6±0.6	7.0±0.4

TABLE 3: TEST MATRIX FOR FREE CORROSION EXPERIMENTS.

	4 hrs.	10 hrs.	24 hrs.	42 hrs.	72 hrs.	192 hrs.
5°C	N/T	N/T	●	●	●	●
RT(~20°C)	N/T	●	●	●	●	N/T
40°C	N/T	●	●	●	●	N/T
65°C	●	●	●	N/T	N/T	N/T

● - Test Performed
N/T - No Test

APPENDIX

PUBLICATIONS FROM THE PROGRAM

D. G. Harlow and R. P. Wei, "A Mechanistically Based Approach to Probability Modeling for Corrosion Fatigue Crack Growth," Engr. Frac. Mech., 45, No. 1, pp. 79-88, 1993.

D. G. Harlow and R. P. Wei, "A Mechanistically Based Probability Approach for Predicting Corrosion and Corrosion Fatigue Life," in ICAF Durability and Structural Integrity of Airframes, Vol. I, A. F. Blom, ed., EMAS, Warley, United Kingdom, pp. 347-366, 1993.

D. Gary Harlow and Robert P. Wei, "A Dominant Flaw Probability Model for Corrosion and Corrosion Fatigue," in Corrosion Control Low-Cost Reliability, 5B, Proceedings of the 12th International Corrosion Congress, Houston, TX, pp. 3573-3586, 1993.

D. Gary Harlow and Robert P. Wei, "A Probability Model for Corrosion and Corrosion Fatigue Life," J. Am. Inst. of Aeronautics and Astronautics, 32, 10, October, 1994, pp. 2073-2079.

G. S. Chen, M. Gao, D. G. Harlow and R. P. Wei, "Corrosion and Corrosion Fatigue of Airframe Aluminum Alloys," FAA/NASA International Symposium on Advanced Structural Integrity Methods for Airframe Durability and Damage Tolerance, NASA Conference Publication 3274, Langley Research Center, Hampton, VA 23681, September 1994, pp.157-173.

Raymond M. Burynski, Jr., "Corrosion Response of a 2024-T3 Alloy in 0.5M NaCl Solution," M.S. Thesis, Lehigh University, 1995.

K.-C. Wan, G. S. Chen, M. Gao and R. P. Wei, "Corrosion Fatigue of a 2024-T3 Aluminum Alloy in the Short Crack Domain," Internatl. J. of Fracture, 69, 3, 1995.

G. S. Chen, M. Gao and R. P. Wei, "Micro-Constituents Induced Pitting Corrosion in a 2024-T3 Aluminum Alloy," Accepted by CORROSION for publication December 1995.

K.-C. Wan, G. S. Chen, M. Gao and R. P. Wei, "Technical Note on The Conventional K-Calibration Equations for Single-Edge-Cracked Tension Specimens," Accepted by Engineering Fracture Mechanics for publication March 1996.

D. G. Harlow, N. R. Cawley and R. P. Wei, "Spatial Statistics of Particles and Corrosion Pits in 2024-T3 Aluminum Alloy," Proceedings of 15th Canadian Congress of Applied Mechanics, B. Tabarrok and S. Dost, eds., May 28-June 2, 1995, Victoria, British Columbia, p. 116, 1995.

Raymond M. Burynski, Jr., Gim-Syang Chen and Robert P. Wei, "Evolution of Pitting Corrosion in a 2024-T3 Aluminum Alloy," 1995 ASME International Mechanical Engineering Congress and Exposition on Structural Integrity in Aging Aircraft, San Francisco, CA, 47, C. I. Chang and C. T. Sun, eds., The American Society of Mechanical Engineers, New York, NY 10017, pp. 175-183, 1995.

D. Gary Harlow and Robert P. Wei, "A Probability Model for the Nucleation and Coalescence of Corrosion Pits in Aluminum Alloys," 1995 ASME International Mechanical Engineering Congress and Exposition on Structural Integrity in Aging Aircraft, San Francisco, CA, 47, C. I. Chang and C. T. Sun, eds., The American Society of Mechanical Engineers, New York, NY 10017, pp. 185-194, 1995.

☆U.S. GOVERNMENT PRINTING OFFICE: 1996 - 704-066/20253